

RESEARCH ARTICLE

# Kinematics of the Hybrid 6-Axis (H6A) manipulator

Pranathi Golla<sup>1,†</sup> , Shashank Ramesh<sup>2,†</sup>  and Sandipan Bandyopadhyay<sup>3</sup> 

<sup>1</sup>Laboratory for Computational Sensing and Robotics, Johns Hopkins University, Baltimore, MD 21218, USA, <sup>2</sup>Department of Aerospace and Mechanical Engineering, University of Notre Dame, Notre Dame, IN 46556, USA, and <sup>3</sup>Department of Engineering Design, Indian Institute of Technology Madras, Chennai 600 036, TN, India

**Corresponding author:** Sandipan Bandyopadhyay; Email: [sandipan@iitm.ac.in](mailto:sandipan@iitm.ac.in)

**Received:** 18 July 2022; **Revised:** 8 February 2023; **Accepted:** 15 February 2023

**Keywords:** hybrid manipulator; forward kinematics; inverse kinematics; inverse kinematic univariate; symbolic computation; closed-form; singularities

## Abstract

This paper presents a comprehensive study of the forward and inverse kinematics of a six-degrees-of-freedom (DoF) spatial manipulator with a novel architecture. Developed by Systemantics India Pvt. Ltd., Bangalore, and designated as the H6A (i.e., Hybrid 6-Axis), this manipulator consists of two arm-like branches, which are attached to a rigid waist at the proximal end and are coupled together via a wrist assembly at the other. Kinematics of the manipulator is challenging due to the presence of two multi-DoF passive joints: a spherical joint in the right arm and a universal in the left. The forward kinematic problem has eight solutions, which are derived analytically in the closed form. The inverse kinematic problem leads to 160 solutions and involves the derivation of a 40-degree polynomial equation, whose coefficients are obtained as closed-form symbolic expressions of the pose parameters of the end-effector, thus ensuring the generality of the results over all possible inputs. Furthermore, the analyses performed lead naturally to the conditions for various singularities involved, including certain non-trivial architecture singularities. The results are illustrated via numerical examples which are validated extensively.

## Nomenclature

|     |  |
|-----|--|
| H6A | Hybrid 6-Axis manipulator                                      |
| DoF | degree(s)-of-freedom   |
| FKP | forward kinematic problem                                      |
| IKP | inverse kinematic problem                                      |
| CAS | computer algebra system  |
| IKU | inverse kinematic univariate (polynomial/equation)             |
| DH  | Denavit–Hartenberg (as in DH parameters, see ref. [1], pp. 43) |

## 1. Introduction

Hybrid manipulators form a class of robots which incorporate some characteristics of both serial and parallel manipulators. The architecture of hybrid manipulators may vary significantly, for instance, it can consist of a sequential concatenation of serial and parallel modules (see, e.g., ref. [2]) or several stages of parallel manipulators arranged in a series (as in ref. [3]) or a parallel combination of serial chains, forming closed kinematic loops (see, e.g., ref. [4]). The main motivation of research into these manipulators is to attain some reasonable compromises between the serial characteristics, for example, large workspaces, and the parallel ones, for example, better payload-to-self-weight ratio, rigidity and superior dynamic response.

Many interesting manipulator architectures of hybrid nature have been proposed and analysed by various researchers in the last few decades. In one of the early works, Waldron *et al.* [2] studied the

<sup>†</sup>These authors contributed to this work as a students of IIT Madras.

kinematics of the ARTISAN hybrid manipulation system whose wrist and micro-manipulator together constitute a six-*degrees-of-freedom* (DoF) serial-parallel module. Spatial robots of six-DoF consisting of two 3-DoF parallel manipulators arranged serially have been analysed by Shahinpoor [3] and Tanev [5]. Romdhane [6] introduced a novel six-DoF “hybrid serial-parallel Stewart like mechanism (HS-PM)”, which also has two 3-DoF parallel manipulators arranged serially. The forward kinematic problem (FKP) of a six-DoF hybrid manipulator with three identical limbs joining a moving platform to the fixed platform is presented in ref. [7]. A two-limbed six-DoF hybrid manipulator, called the *Hybrid 6-Axis Articulated Robot* (H6AR), has been developed by Systemantics India Pvt. Ltd., Bangalore, and its kinematics has been analysed in ref. [8]. Chablat *et al.* [4] have discussed the kinematic properties of a three-DoF hybrid manipulator capable of avoiding gain-type singularities. The stiffness characteristics of a novel hybrid manipulator called the Cassino Hybrid Manipulator (CaHyMan) has been investigated analytically in the *closed form* in ref. [9]. Forward kinematics of a serial chain of 3-UPS manipulators was analysed by means of screw theory in ref. [10]. Screw theory was employed in ref. [11] to study the forward kinematics of the hybrid manipulator IRB 260 developed by the company ABB, as well as the mobility of another six-DoF spatial hybrid manipulator in ref. [12]. The latter manipulator, consisting of two spatial parallel manipulators in series, has been analysed recently by Hu *et al.* [13] with regard to its inverse kinematics. Furthermore, the statics and stiffness characteristics of hybrid manipulators consisting of  $k$ -stages of parallel manipulators arranged serially have been investigated by Hu *et al.* [14].

Several studies have been conducted on the kinematics of five-DoF hybrid manipulators designed as serial combinations of a three-DoF parallel manipulator and a two-DoF serial manipulator. For instance, Guo *et al.* [15] have presented the closed-form kinematics of a novel hybrid manipulator, which consists of a 3T parallel module and a 2-R serial module. This 3T2R manipulator was modelled mathematically using *Denavit–Hartenberg* (DH) parameters. The inverse kinematics of a 2-R serial manipulator mounted on a 2R1T parallel manipulator is discussed in ref. [16]. Similarly, the forward and inverse kinematics of a combination of a 2-UPU parallel manipulator and a 2-R serial manipulator are studied in ref. [17]. The forward and inverse kinematics of a 3T2R parallel-serial (hybrid) manipulator are presented in ref. [18]. Yet another 5-axis hybrid robot, the TriMule, was analysed for its inverse kinematics and singularities in ref. [19].

The applications of hybrid manipulators have also been as varied as their architectures. For instance, Yang *et al.* have presented closed-form symbolic solutions for both the forward and inverse kinematics of a new six-DoF hybrid manipulator with applications in deburring tasks for large jet-engine components in ref. [20]. Xu *et al.* [21] described the design of a hybrid manipulator, which is composed of a three-DoF parallel module, a two-DoF serial module and a redundant DoF, to aid in the process of computer-controlled ultra-precision free-form polishing. Inverse kinematic analysis of a new hybrid manipulator used for medical purposes was presented in ref. [22]. This manipulator was formed by the serial combination of a three-DoF SCARA and a Stewart platform manipulator. Singh *et al.* [23] studied the kinematics of a seven-DoF spatial hybrid manipulator, meant to aid in surgery. Both the manipulators described in refs. [22, 23] were modelled using DH parameters.

This paper presents a detailed analysis of the kinematics of a novel six-DoF spatial hybrid manipulator, namely the *Hybrid 6-Axis* (H6A), developed by Systemantics India Pvt. Ltd., Bangalore. The manipulator consists of a pair of two-DoF serial arms arranged in parallel vertical planes (see Fig. 1). These are mounted on a rigid “waist”, which itself can rotate about a vertical axis fixed to the inertial frame of reference. At the other end, the arms are joined via a wrist assembly, thus creating a closed loop. At the wrist, the yaw and roll<sup>1</sup> DoFs are produced by the closed chain, while an actuator mounted on the wrist is responsible for a pitch motion, which is independent of the rest of the manipulator. The *FKP* and the *inverse kinematic problem* (IKP) of the manipulator are studied comprehensively in the closed form

<sup>1</sup>In this paper, the yaw, roll and pitch motions at the end-effector of the manipulator have been defined w.r.t. the inertial frame of reference, when  $\theta_1 = 0$ .

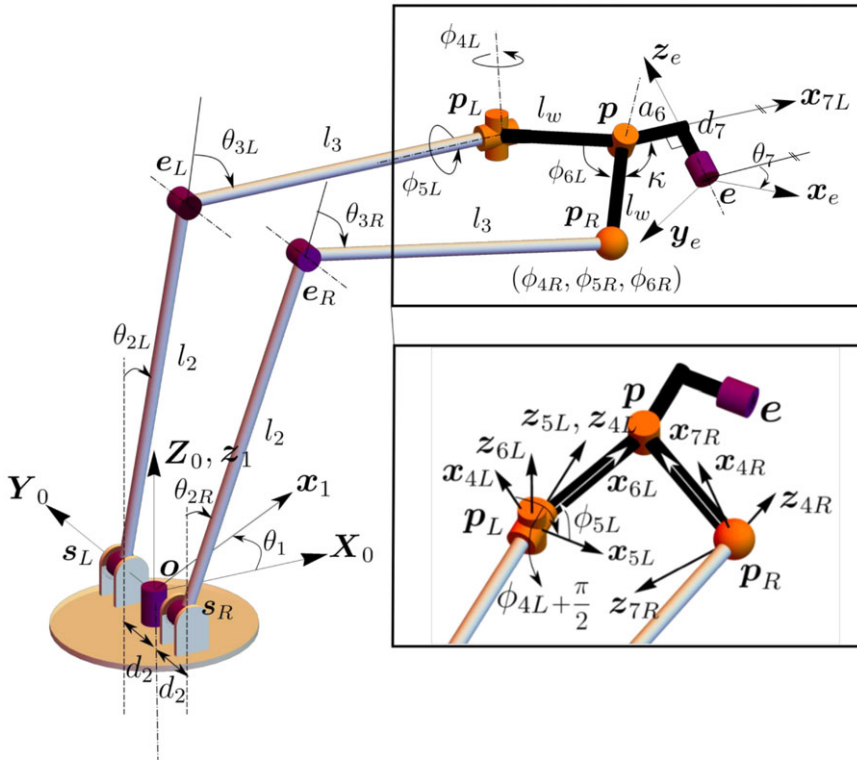


**Figure 1.** Kinematic diagram of the H6A manipulator, showing the reference frames associated with the passive joints in additional close-ups.

using extensive symbolic computations in a *computer algebra system* (CAS).<sup>2</sup> It is established that the solution to the FKP has eight branches (including the complex ones, if any) for a generic set of actuator inputs. Interestingly, even when all the branches are real, they manifest only as two identical sets of four *poses*<sup>3</sup> physically, as a pair of distinct values of joint angles at the passive spherical joint on the right arm lead to the same configuration of the robot (see Fig. 2). The solution of the IKP turns out to be much more complicated and interesting, which involves the derivation and solution of a 40-degree univariate polynomial equation. For each solution of the said equation, there are four possible configurations of the manipulator (including the complex ones, as the case may be), thus leading to a total of 160 solutions in the general case. The solution procedure is illustrated numerically, and the results thereof are validated by checking the residues of the original set of constraint equations, as well as comparing the solutions of IKP with the corresponding inputs of the forward kinematics. Singularities associated with the FKP and IKP are identified using the general condition of the merger of the branches of solutions. These are further analysed to identify the corresponding loss and gain of DoF(s) at the end-effector of the manipulator.

The key contributions of this paper may be summarised as follows.

The primary contribution of this work is to solve the kinematics of a hybrid manipulator with a novel architecture. The topology of H6A is unique, and any such “twin-handed” yet asymmetric hybrid architecture has not been analysed before, to the best of the authors’ knowledge. The nature of the analysis is *exact* and comprehensive, as opposed to numerical and consequently, partial. Due to the

<sup>2</sup>In this paper, the CAS Mathematica v12.0 has been used for all symbolic as well as numeric computations.

<sup>3</sup>The pose of a rigid body refers to the combination of its position and orientation.

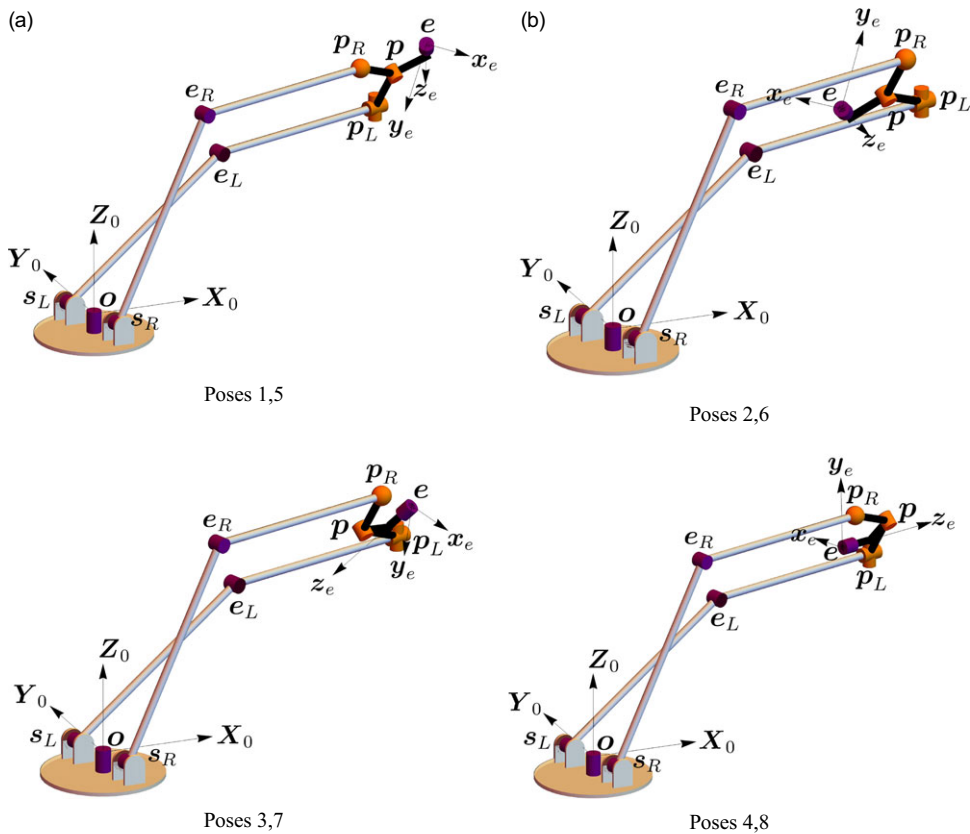


**Figure 2.** Poses depicting the solutions to the forward kinematic problem for the given inputs (enumerated as per the rows of Table IV).

exact analytical nature of this work, the total number of solutions is *conclusively* established. The final results do not contain any spurious components and are, therefore, *provably minimal*. Furthermore, the symbolic nature of the kinematic analysis makes it easy to perform extensive analytical studies of the singularities. For example, a condition on the architecture parameters, which would lead to finite self-motion, was derived in the closed form (see Eq. (90)), along with other conditions for singularities.

A secondary contribution of the paper lies in the more generic field of symbolic computations. A number of techniques were developed and utilised in a fruitful manner to derive the analytical results presented in this paper (as detailed in Section 7). These techniques may be applied to any other problem in kinematics and beyond.

Finally, the *integrated approach* towards kinematics, which encompasses position and singularity analysis in the *exact closed form*, is a major contribution of this work, as its scope of application is not limited to this manipulator or even just hybrid manipulators – it could be applied to manipulators of *any* architecture, at least in principle. That it was applicable in the case of such a complex spatial hybrid manipulator establishes this claim in an objective manner.

The remainder of this paper is organised as follows: Section 2 presents the kinematic model of the manipulator, from the geometrical description of the manipulator to the derivation of the loop-closure equations. Sections 3 and 4 contain the detailed solution procedures of the FKP and IKP, respectively. Section 5 presents the numerical examples, including the validation of the results. The singularities of the manipulator mentioned above are studied in Section 6. The formulations and results presented in the paper are summarised in Section 7. Finally, the conclusions are presented in Section 8.

## 2. Kinematic model of the manipulator

The geometry of the H6A manipulator is described in this section, followed by the derivation of the loop-closure equations.

### 2.1. Geometry

The kinematic sketch of the H6A manipulator is shown in Fig. 1. The global frame of reference,  $X_0Y_0Z_0$ , is attached to the waist joint,  $o$ , which rotates about the  $Z_0$  axis. The robot manipulator is composed of a pair of 2-R “arms”,  $s_L e_L - e_L p_L$  on the left and  $s_R e_R - e_R p_R$  on the right, both of which are attached to the waist at a fixed offset  $d_2$  from the centre of the waist,  $o$ . The left arm comprises an upper arm,  $s_L e_L$ , of length  $l_2$  and a forearm,  $e_L p_L$ , of length  $l_3$ . Similarly, the right arm consists of an upper arm,  $s_R e_R$ , and a forearm,  $e_R p_R$ , of lengths  $l_2$  and  $l_3$ , respectively. At the other end, the serial arms are connected together via a wrist assembly,  $p_L - p - p_R$ . The left arm is attached to the wrist assembly through a universal joint located at  $p_L$ . Likewise, a spherical at  $p_R$  joins the right arm and the wrist assembly. The wrist assembly itself consists of two links of length  $l_w$ , which connect each arm to a rotary joint located at the *wrist point*,  $p$ . Additionally, an end-effector,  $e$ , is connected to the rotary joint at  $p$ , through an L-shaped link having proximal and distal arms of lengths  $a_6$  and  $d_7$ , respectively. Thereafter, the L-shaped link is joined to the link  $p_R p$  at an angle  $\kappa$ . While the closed loop  $o - s_L - e_L - p_L - p - p_R - e_R - s_R - o$  is responsible for the yaw and roll motions at the end-effector, a revolute actuator placed right before the end-effector is responsible for the pitch motion which is decoupled from the rest of the motions of the manipulator.

The waist joint at  $o$ , shoulder joints at  $s_L$  and  $s_R$ , elbow joints at  $e_L$  and  $e_R$  and the revolute joint situated before the end-effector,  $e$ , are *active* (i.e., actuated), and the corresponding joint angles are denoted by  $\theta_1, \theta_{2L}, \theta_{2R}, \theta_{3L}, \theta_{3R}$  and  $\theta_7$ , respectively. These joints account for the six-DoF of the end-effector.<sup>4</sup> On the other hand, the joints associated with the wrist assembly, that is, those located at  $p_L, p$  and  $p_R$ , respectively, are *passive* (i.e., unactuated), and the corresponding joint angles are  $\{\phi_{4L}, \phi_{5L}\}, \phi_{6L}$  and  $\{\phi_{4R}, \phi_{5R}, \phi_{6R}\}$ , respectively. Figure 1 shows the references for all the pertinent joint angles. For instance, the angle  $\theta_1$  is measured as the angle between  $X_0$  and  $x_1$ , measured about  $Z_0$ . Similarly,  $\theta_7$  is the angle that  $x_e$  makes with (a line parallel to)  $x_{7L}$ . The close-ups of the wrist in Fig. 1 depict the frames<sup>5</sup> associated with the universal joint at  $p_L$  and spherical joint  $p_R$ . The intermediate frames at the spherical joint are omitted to avoid clutter. The rotation at the spherical joint  $p_R$ , between the frames  $x_{4R} z_{4R} y_{4R}$  and  $x_{7R} y_{7R} z_{7R}$  (the axes  $y_{4R}, y_{7R}$  being omitted in the figure) may be represented using the **ZZZ** convention of Euler angles as  $R_Z(\phi_{4R})R_X(\phi_{5R})R_Z(\phi_{6R} + \pi/2)$ . In summary, the H6A manipulator has a total of seven architecture parameters, namely  $\{d_2, l_2, l_3, l_w, a_6, d_7, \kappa\}$ , and six actuated joints represented by the active angles,  $\theta = [\theta_1, \theta_{2L}, \theta_{2R}, \theta_{3L}, \theta_{3R}, \theta_7]^T$ . In addition, there are six joints represented by the passive angles,  $\phi = [\phi_{4L}, \phi_{4R}, \phi_{5L}, \phi_{5R}, \phi_{6L}, \phi_{6R}]^T$ . The *left kinematic chain* of the manipulator starts at the waist,  $o$ , and runs all the way to the end-effector,  $e$ , via the left elbow; it is designated as  $o - s_L - e_L - p_L - p - e$ . Similarly, the *right chain*, running from  $o$  to  $p$ , is designated as  $o - s_R - p - e_R - p_R - p$ . In order to keep the kinematic descriptions of these chains simple and generic, these are described via the DH parameters (see, e.g., ref. [1], pp. 43) owing primarily to the universal popularity of this system. The left and right chains are described in Tables I and II, respectively.<sup>6</sup> Further, from these tables, two sequences of  $4 \times 4$  homogeneous transformation matrices, namely  ${}^0_1T, \dots, {}^7_8T_L$  and  ${}^0_1T, \dots, {}^7_8T_R$ , are generated in a systematic manner, which are subsequently used in Section 2.2 to formulate the loop-closure equations of the manipulator.

It may be noted here that the architecture of the H6A is unique in the sense that it resembles two hands emanating separately from a single-DoF “waist”, which are brought back together at the wrist assembly. An additional and independently actuated link attached to the wrist assembly constitutes the final output. The remaining four-DoF appear in the portion of the manipulator where the two arms

<sup>4</sup>The DoF of the manipulator is calculated in Appendix A following [30].

<sup>5</sup>The naming convention of the frames follows that of the transformation matrices listed in Tables I and II.

<sup>6</sup>All the angles are measured CCW about the respective axes of rotation.

**Table I.** DH parameters for the left chain of the H6A manipulator.

| $i$ | Transformation matrix | $\alpha_{i-1}$   | $a_{i-1}$ | $d_i$  | $\theta_i$                    | Origin of the $(i-1)^{\text{th}}$ frame |
|-----|-----------------------|------------------|-----------|--------|-------------------------------|---|
| 1   | ${}^0_1\mathbf{T}$    | 0                | 0         | 0      | $\theta_1$                    | Global frame, $X_0Y_0Z_0$               |
| 2   | ${}^1_2\mathbf{T}_L$  | $-\frac{\pi}{2}$ | 0         | $d_2$  | $\theta_{2L} - \frac{\pi}{2}$ | Waist, $\mathbf{o}$                     |
| 3   | ${}^2_3\mathbf{T}_L$  | 0                | $l_2$     | 0      | $\theta_{3L} - \frac{\pi}{2}$ | Left shoulder, $s_L$                    |
| 4   | ${}^3_4\mathbf{T}_L$  | $-\frac{\pi}{2}$ | 0         | $l_3$  | 0                             | Left elbow, $e_L$                       |
| 5   | ${}^4_5\mathbf{T}_L$  | 0                | 0         | 0      | $\phi_{4L} + \frac{\pi}{2}$   |   |
| 6   | ${}^5_6\mathbf{T}_L$  | $\frac{\pi}{2}$  | 0         | 0      | $\phi_{5L}$                   | Universal joint, $p_L$                  |
| 7   | ${}^6_7\mathbf{T}_L$  | 0                | $l_w$     | 0      | $\kappa + \phi_{6L} - \pi$    |   |
| 8   | ${}^7_8\mathbf{T}_L$  | $-\frac{\pi}{2}$ | $a_6$     | $-d_7$ | $\theta_7$                    | Wrist point, $\mathbf{p}$               |

**Table II.** DH parameters for the right chain of the H6A manipulator.

| $i$ | Transformation matrix | $\alpha_{i-1}$   | $a_{i-1}$ | $d_i$  | $\theta_i$                    | Origin of the $(i-1)^{\text{th}}$ frame |
|-----|-----------------------|------------------|-----------|--------|-------------------------------|---|
| 1   | ${}^0_1\mathbf{T}$    | 0                | 0         | 0      | $\theta_1$                    | Global frame, $X_0Y_0Z_0$               |
| 2   | ${}^1_2\mathbf{T}_R$  | $-\frac{\pi}{2}$ | 0         | $-d_2$ | $\theta_{2R} - \frac{\pi}{2}$ | Waist, $\mathbf{o}$                     |
| 3   | ${}^2_3\mathbf{T}_R$  | 0                | $l_2$     | 0      | $\theta_{3R} - \frac{\pi}{2}$ | Left shoulder, $s_R$                    |
| 4   | ${}^3_4\mathbf{T}_R$  | $-\frac{\pi}{2}$ | 0         | $l_3$  | 0                             | Left elbow, $e_R$                       |
| 5   | ${}^4_5\mathbf{T}_R$  | 0                | 0         | 0      | $\phi_{4R} + \frac{\pi}{2}$   |   |
| 6   | ${}^5_6\mathbf{T}_R$  | $\frac{\pi}{2}$  | 0         | 0      | $\phi_{5R}$                   | Spherical joint, $p_R$                  |
| 7   | ${}^6_7\mathbf{T}_R$  | $-\frac{\pi}{2}$ | 0         | 0      | $\phi_{6R}$                   |   |
| 8   | ${}^7_8\mathbf{T}_R$  | $\frac{\pi}{2}$  | $l_w$     | 0      | $\kappa - \pi$                |   |

are not connected to each other. As such, it may be but natural to expect that these parts of the two arms, that is,  $s_L$ - $e_L$ - $p_L$  and  $s_R$ - $e_R$ - $p_R$ , should be identical in their architecture, inclusive of the manner at which they meet the wrist assembly. Indeed, this thought process seems to have led to the design of the manipulator H6AR, introduced in ref. [8], which preceded the manipulator H6A. However, the output DoF of the H6AR manipulator, based on its architecture, is seen to be *five*, that is, given its six actuators, the manipulator is *redundantly actuated*. The design of H6A eliminates this problem by replacing one of the two universal joints connecting the arms to the wrist assembly by a spherical joint (at  $p_R$ , to be specific), while retaining the symmetry in the rest of the architecture, as well as in the dimensions of the individual links.<sup>7</sup> Evidently, this asymmetric architecture leads to interesting kinematic behaviours, as may be seen in Section 4, in particular.

<sup>7</sup>It may be noted here that if both the universal joints in the H6A manipulator were to be replaced by spherical joints, in order to maintain complete symmetry between the two arms, the manipulator would have become *kinematically redundant*, and *under-actuated*, having seven-DoF and six actuators.

**2.2. Loop-closure equations**

The loop-closure equations are constraints which ensure that the manipulator maintains its kinematic integrity at every configuration. For the manipulator at hand, these equations are formulated by equating the pose of the wrist point  $p$  calculated through the left chain with that from the right. Hence, the transformation matrix  ${}^0_pT \in SE(3)$  is determined as a concatenation of the matrices in constituting the second column of Table I using the left chain (see, e.g., ref. [1], pp. 48):

$${}^0_pT = {}^0_1T {}^1_2T {}^2_3T {}^3_4T {}^4_5T {}^5_6T {}^6_7T. \tag{1}$$

The matrix  ${}^0_pT$  may also be computed considering the right chain (refer to Table II):

$${}^0_pT = {}^0_1T {}^1_2T {}^2_3T {}^3_4T {}^4_5T {}^5_6T {}^6_7T {}^7_8T. \tag{2}$$

Therefore, the loop-closure constraints are obtained by equating the expressions of  ${}^0_pT$  appearing in Eqs. (1) and (2) and eliminating the common factor,  ${}^0_1T$ , between them:

$${}^1_2T {}^2_3T {}^3_4T {}^4_5T {}^5_6T {}^6_7T = {}^1_2T {}^2_3T {}^3_4T {}^4_5T {}^5_6T {}^6_7T {}^7_8T. \tag{3}$$

Equation (3) contains six independent scalar equations, which form the loop-closure equations of the manipulator. The six unknown passive joint angles,  $\phi$ , are solved in terms of the active joint angles,  $\theta$ , in the next section.

**3. Forward kinematics**

The FKP is defined as the determination of the poses of end-effector of the H6A manipulator, as represented via:

$${}^0_eT = {}^0_pT {}^p_eT \in SE(3), \tag{4}$$

for a given set of active joint angle inputs,  $\theta$ . It involves an intermediary step of solving for the passive joint angle variables,  $\phi$ , in terms of the active joint angle inputs,  $\theta$ .

Firstly, the loop-closure constraint, (3), is rearranged to obtain the passive joint angle variables corresponding to the left chain, grouped together as  $\phi_L = [\phi_{4L}, \phi_{5L}, \phi_{6L}]^T$ :

$${}^4_5T {}^5_6T {}^6_7T {}^7_8T ({}^8T_R)^{-1} = ({}^1_2T {}^2_3T {}^3_4T)^{-1} {}^1_2T {}^2_3T {}^3_4T {}^4_5T {}^5_6T {}^6_7T. \tag{5}$$

Subsequently, equating the displacement vectors (i.e., the first three rows of the fourth column) on both sides of (5) yields

$$\eta_{FKL} := 2l_w \sin \frac{\phi_{6L}}{2} \begin{bmatrix} -\sin \phi_{4L} \sin \left( \phi_{5L} + \frac{\phi_{6L}}{2} \right) \\ \cos \phi_{4L} \sin \left( \phi_{5L} + \frac{\phi_{6L}}{2} \right) \\ -\cos \left( \phi_{5L} + \frac{\phi_{6L}}{2} \right) \end{bmatrix} - \begin{bmatrix} l_{13} \\ l_{23} \\ l_{33} \end{bmatrix} = \mathbf{0}, \text{ where:}$$

$$\alpha_1 = \theta_{2L} - \theta_{2R} + \theta_{3L} - \theta_{3R},$$

$$l_{13} = -l_2 \sin \theta_{3L} + l_2 \sin (\alpha_1 + \theta_{3R}) + l_3 \sin \alpha_1,$$

$$l_{23} = 2d_2,$$

$$l_{33} = -l_2 \cos \theta_{3L} + l_2 \cos (\alpha_1 + \theta_{3R}) - l_3 (1 - \cos \alpha_1). \tag{6}$$

The forward kinematic univariate equation, in  $\phi_{6L}$ , may be obtained as:

$$4l_w^2 \sin^2 \left( \frac{\phi_{6L}}{2} \right) - (l_{13}^2 + l_{23}^2 + l_{33}^2) = 0. \tag{7}$$

Equation (7) yields, in general, four distinct values of  $\frac{\phi_{6L}}{2}$ , given by:

$$\frac{\phi_{6L}}{2} = \arcsin\left(\frac{\pm\sqrt{l_{13}^2 + l_{23}^2 + l_{33}^2}}{2l_w}\right), \quad \pi - \arcsin\left(\frac{\pm\sqrt{l_{13}^2 + l_{23}^2 + l_{33}^2}}{2l_w}\right), \text{ since } l_w \neq 0. \tag{8}$$

However, these solutions coalesce into only a pair of distinct solutions for  $\phi_{6L}$  (since  $2\pi \pm \psi \equiv \pm\psi$ ,  $\forall \psi \in [0, 2\pi]$ ):

$$\phi_{6L} = \pm 2 \arcsin\left(\frac{\sqrt{l_{13}^2 + l_{23}^2 + l_{33}^2}}{2l_w}\right). \tag{9}$$

The remaining unknowns in (6) are obtained as:<sup>8</sup>

$$\phi_{5L} = \text{atan2}\left(\frac{\pm\sqrt{l_{13}^2 + l_{23}^2}}{2l_w \sin \frac{\phi_{6L}}{2}}, \frac{-l_{33}}{2l_w \sin \frac{\phi_{6L}}{2}}\right) - \frac{\phi_{6L}}{2}, \text{ assuming } \sin \frac{\phi_{6L}}{2} \neq 0; \tag{10}$$

$$\phi_{4L} = \text{atan2}\left(\frac{-l_{13}}{2l_w \sin\left(\phi_{5L} + \frac{\phi_{6L}}{2}\right) \sin \frac{\phi_{6L}}{2}}, \frac{l_{23}}{2l_w \sin\left(\phi_{5L} + \frac{\phi_{6L}}{2}\right) \sin \frac{\phi_{6L}}{2}}\right),$$

assuming further:  $\sin\left(\phi_{5L} + \frac{\phi_{6L}}{2}\right) \neq 0.$  (11)

It may be observed from Eqs. (9)–(11) that there are *four*<sup>9</sup> distinct sets of solutions for the passive joint angles  $\phi_L$  for a generic input. However, under special conditions these solutions can merge, for example, when  $l_{13}^2 + l_{23}^2 + l_{33}^2 = 0 \Rightarrow \sin \frac{\phi_{6L}}{2} = 0$ , or  $l_{13}^2 + l_{23}^2 = 0 \Rightarrow \sin\left(\phi_{5L} + \frac{\phi_{6L}}{2}\right) = 0$ , Eqs. (9) and (10) have repeated real solutions due to the coalescence of pairs of real or complex conjugate solutions, which then manifest as pairs of coincident real solutions, thus forming the boundaries between the real and complex solutions. These singular cases are discussed in Case 1 in Section 6.1.

The unknown passive joint variables associated with the right arm, namely  $\phi_R = [\phi_{4R}, \phi_{5R}, \phi_{6R}]^T$ , are solved in a manner similar to the analysis of the left arm described above. First, the loop-closure equation, (3), is rearranged as:

$${}^4T_R {}^5T_R {}^6T_R {}^7T_R = ({}^1T_R {}^2T_R {}^3T_R {}^4T_R)^{-1} {}^1T_L {}^2T_L {}^3T_L {}^4T_L {}^5T_L {}^6T_L {}^7T_L ({}^8T_R)^{-1}. \tag{12}$$

Thereafter, equating elements (1, 3), (2, 3), (3, 1), (3, 2) and (3, 3) of the transformation matrices (where element  $(i, j)$  appears in the  $i$ th row and the  $j$ th column of a matrix) appearing on either side of (12), one obtains

$$\eta_{FKR} := \begin{bmatrix} \sin \phi_{4R} \sin \phi_{5R} \\ -\cos \phi_{4R} \sin \phi_{5R} \\ \cos \phi_{5R} \\ \cos \phi_{6R} \sin \phi_{5R} \\ -\sin \phi_{6R} \sin \phi_{5R} \end{bmatrix} - \begin{bmatrix} r_{13} \\ r_{23} \\ r_{33} \\ r_{31} \\ r_{32} \end{bmatrix} = \mathbf{0}, \text{ where:} \tag{13}$$

<sup>8</sup>In the above,  $\text{atan2}(a \sin(\cdot), a \cos(\cdot))$ ,  $a \in \mathbb{R}$ , denotes the *two-argument arctangent* function.

<sup>9</sup>It may appear that the total number of solutions is eight, if one considers (8) instead of (9). This anomaly is akin to a *parametric singularity* which is of no consequence to the kinematics of the physical manipulator and its configurations corresponding to a given set of inputs.

$$\begin{aligned} \beta_1 &= \phi_{5L} + \phi_{6L}, \\ r_{13} &= \frac{1}{4}(\cos(\alpha_1 + \phi_{4L} - \beta_1) - \cos(\alpha_1 - \phi_{4L} - \beta_1) + \cos(\alpha_1 - \phi_{4L} + \beta_1) - \cos(\alpha_1 + \phi_{4L} + \beta_1) \\ &\quad - 2 \sin(\alpha_1 - \beta_1) + 2 \sin(\alpha_1 + \beta_1)), \\ r_{23} &= -\cos \phi_{4L} \sin \beta_1, \\ r_{33} &= \frac{1}{2}(\cos(\alpha_1 - \beta_1) + \cos(\alpha_1 + \beta_1) + 2 \sin \alpha_1 \sin \phi_{4L} \sin \beta_1), \\ r_{31} &= \frac{1}{4}(\cos(\alpha_1 + \phi_{4L} - \beta_1) - \cos(\alpha_1 - \phi_{4L} - \beta_1) - \cos(\alpha_1 - \phi_{4L} + \beta_1) + \cos(\alpha_1 + \phi_{4L} + \beta_1) \\ &\quad - 2 \sin(\alpha_1 - \beta_1) + 2 \sin(\alpha_1 + \beta_1)), \\ r_{32} &= -\cos \phi_{4L} \sin \alpha_1. \end{aligned}$$

The passive joint angles  $\phi_L$  have been obtained previously, as in Eqs. (9)–(11). Taking these into cognisance, the solutions of passive angles  $\phi_R$  from (13) are computed as:

$$\phi_{5R} = \text{atan2} \left( \pm \sqrt{r_{31}^2 + r_{32}^2}, r_{33} \right), \tag{14}$$

$$\phi_{4R} = \text{atan2} \left( \frac{r_{13}}{\sin \phi_{5R}}, \frac{-r_{23}}{\sin \phi_{5R}} \right), \text{ assuming } \sin \phi_{5R} \neq 0; \tag{15}$$

$$\phi_{6R} = \text{atan2} \left( \frac{-r_{32}}{\sin \phi_{5R}}, \frac{r_{31}}{\sin \phi_{5R}} \right), \text{ assuming } \sin \phi_{5R} \neq 0. \tag{16}$$

Equations (14)–(16) show that the passive joint angles  $\phi_R$  have two solutions for a generic set of passive joint angles  $\phi_L$ . These solutions merge when  $r_{31}^2 + r_{32}^2 = 0 \Rightarrow \sin \phi_{5R} = 0$ , (14) produces repeated roots. This singularity is studied in Case 2 of Section 6.1.

After computing the solutions of  $\phi_L$  from Eqs. (9)–(11) and those of  $\phi_R$  from Eqs. (14)–(16), the configurations of all the links may be ascertained from the link-transformation matrices given in Tables I and II, thus completing the solution of the FKP. The total number of solutions to the FKP for any generic input equals  $4 \times 2 = 8$  (see Table IV and Fig. 2 in Section 5.1).

The solution procedure for the IKP is presented in the following section.

#### 4. Inverse kinematics

The IKP involves the determination of the active joint angles,  $\theta$ , along with the passive joint angles,  $\phi$ , for a given pose of the end-effector of the H6A manipulator, as represented by the matrix  ${}^0_eT \in \mathbb{SE}(3)$ . The task-space coordinates are input in the form of a displacement vector,  $\mathbf{p} = [p_x, p_y, p_z]^T$ , and three Euler angles, namely  $\{\alpha, \beta, \gamma\}$ , representing the orientation of the end-effector in the ZYZ convention, leading to the following parametrisation of the task space:

$${}^0_eT = \begin{bmatrix} \mathbf{R}_{ZYZ} & \mathbf{p} \\ \mathbf{0}_{1 \times 3} & 1 \end{bmatrix}, \text{ where } \mathbf{R}_{ZYZ} := \mathbf{R}_Z(\alpha)\mathbf{R}_Y(\beta)\mathbf{R}_Z(\gamma) \in \mathbb{SO}(3). \tag{17}$$

In (17),  $\mathbf{R}_Z(\alpha) \in \mathbb{SO}(3)$  (i.e., the *special orthogonal group of three dimensions*) is the rotation matrix corresponding to a CCW rotation about the positive  $Z$  axis by an angle  $\alpha$ , and so on. For the sake of convenience, the following variables are introduced, which are combinations of previously defined joint angles, Euler angles and architecture parameters:

$$\theta_{23L} := \theta_{2L} + \theta_{3L}, \quad \psi_{6L} := \phi_{6L} + \kappa, \quad \theta_{\alpha_1} := \alpha - \theta_1, \quad \theta_{\gamma_7} := \gamma - \theta_7, \quad \theta_{23R} := \theta_{2R} + \theta_{3R}.$$

The poses of the end-effector expressed through the left and the right chains, that is, using (1) and (2), are used for solving the IKP. The pose of the end-effector can be described using (4). Rewriting (4) using (1), that is, the pose of the end-effector considering the left chain, leads to:

$$({}^0_1T)^{-1} {}^0_eT ({}^4_5T_L {}^5_6T_L {}^6_7T_L {}^7_8T_L)^{-1} = {}^1_2T_L {}^2_3T_L {}^3_4T_L. \tag{18}$$

The three components of the displacement vectors on both sides of (18) are equated to obtain:

$$\eta_{1L} := l_2 \sin \theta_{2L} + l_3 \sin \theta_{23L} - p_x \cos(\alpha - \theta_{\alpha_1}) - p_y \sin(\alpha - \theta_{\alpha_1}) - (d_7 - l_w \sin \psi_{6L}) \cos \theta_{\alpha_1} \sin \beta + (a_6 - l_w \cos \psi_{6L})(\cos \beta \cos \theta_{\alpha_1} \cos \theta_{\gamma_7} - \sin \theta_{\alpha_1} \sin \theta_{\gamma_7}) = 0, \tag{19}$$

$$\eta_{2L} := d_2 - p_y \cos(\alpha - \theta_{\alpha_1}) + p_x \sin(\alpha - \theta_{\alpha_1}) - (d_7 - l_w \sin \psi_{6L}) \sin \beta \sin \theta_{\alpha_1} + (a_6 - l_w \cos \psi_{6L})(\cos \beta \cos \theta_{\gamma_7} \sin \theta_{\alpha_1} + \cos \theta_{\alpha_1} \sin \theta_{\gamma_7}) = 0, \tag{20}$$

$$\eta_{3L} := l_2 \cos \theta_{2L} + l_3 \cos \theta_{23L} - p_z - (a_6 - l_w \cos \psi_{6L}) \sin \beta \cos \theta_{\gamma_7} - (d_7 - l_w \sin \psi_{6L}) \cos \beta = 0. \tag{21}$$

Additionally, equating the elements (1,3), (3,2) and (3,3) of the rotation matrices on both sides of (18) leads to the following equations:

$$\xi_{1L} := \sin \theta_{23L} + \cos(\phi_{5L} + \psi_{6L}) \sin \beta \cos \theta_{\alpha_1} + \sin(\phi_{5L} + \psi_{6L})(\cos \beta \cos \theta_{\gamma_7} \cos \theta_{\alpha_1} - \sin \theta_{\alpha_1} \sin \theta_{\gamma_7}) = 0, \tag{22}$$

$$\xi_{2L} := \cos \theta_{23L} + \cos \beta \cos(\phi_{5L} + \psi_{6L}) - \sin \beta \cos \theta_{\gamma_7} \sin(\phi_{5L} + \psi_{6L}) = 0, \tag{23}$$

$$\xi_{3L} := \sin \phi_{4L} \sin \beta \sin \theta_{\gamma_7} - \cos \phi_{4L}(\sin \beta \cos(\phi_{5L} + \psi_{6L}) \cos \theta_{\gamma_7} + \cos \beta \sin(\phi_{5L} + \psi_{6L})) = 0. \tag{24}$$

Equations (19)–(24) are functions of the seven unknown variables appearing in the left chain, that is,  $\mathbf{q}_L = [\theta_{\alpha_1}, \theta_{2L}, \theta_{23L}, \phi_{4L}, \phi_{5L}, \psi_{6L}, \theta_{\gamma_7}]^\top$ .

Similarly, rewriting (4) using (2), that is, the pose of the end-effector expressed through the right chain, yields

$$({}^0\mathbf{T})^{-1} {}^0_e\mathbf{T} ({}^4_5\mathbf{T}_R {}^5_6\mathbf{T}_R {}^6_7\mathbf{T}_R {}^7_8\mathbf{T}_R {}^8\mathbf{T}_L)^{-1} = {}^1_2\mathbf{T}_R {}^2_3\mathbf{T}_R {}^3_4\mathbf{T}_R. \tag{25}$$

Equating the three elements of the displacement vector on both sides of (25) produces

$$\eta_{1R} := l_2 \sin \theta_{2R} + l_3 \sin \theta_{23R} - (d_7 - l_w \sin \kappa) \cos \theta_{\alpha_1} \sin \beta - p_x \cos(\alpha - \theta_{\alpha_1}) - p_y \sin(\alpha - \theta_{\alpha_1}) + (a_6 - l_w \cos \kappa)(\cos \beta \cos \theta_{\alpha_1} \cos \theta_{\gamma_7} - \sin \theta_{\alpha_1} \sin \theta_{\gamma_7}) = 0, \tag{26}$$

$$\eta_{2R} := d_2 - p_x \sin(\alpha - \theta_{\alpha_1}) + p_y \cos(\alpha - \theta_{\alpha_1}) + (d_7 - l_w \sin \kappa) \sin \beta \sin \theta_{\alpha_1} - (a_6 - l_w \cos \kappa)(\cos \theta_{\alpha_1} \sin \theta_{\gamma_7} + \cos \beta \sin \theta_{\alpha_1} \cos \theta_{\gamma_7}) = 0, \tag{27}$$

$$\eta_{3R} := l_2 \cos \theta_{2R} + l_3 \cos \theta_{23R} - (a_6 - l_w \cos \kappa) \sin \beta \cos \theta_{\gamma_7} - (d_7 - l_w \cos \kappa) \cos \beta - p_z = 0. \tag{28}$$

Moreover, the elements (1,3), (2,3) and (3,2) of the rotation matrices on both sides of (25) are equated to obtain:

$$\xi_{1R} := \sin \theta_{23R} - \sin \theta_{\alpha_1} (\cos \phi_{5R} \sin \theta_{\gamma_7} \sin \kappa + \sin \phi_{5R} (\cos \kappa \cos \phi_{6R} \sin \theta_{\gamma_7} + \cos \theta_{\gamma_7} \sin \phi_{6R})) + \cos \theta_{\alpha_1} (\cos \beta (\sin \kappa \cos \phi_{5R} \cos \theta_{\gamma_7} - \sin \phi_{5R} (\sin \phi_{6R} \sin \theta_{\gamma_7} - \cos \kappa \cos \phi_{6R} \cos \theta_{\gamma_7})) - \sin \beta (\sin \kappa \sin \phi_{5R} \cos \phi_{6R} - \cos \kappa \cos \phi_{5R})) = 0, \tag{29}$$

$$\xi_{2R} := \cos \theta_{\alpha_1} (\sin \phi_{5R} (\cos \kappa \cos \phi_{6R} \sin \theta_{\gamma_7} + \cos \theta_{\gamma_7} \sin \phi_{6R}) + \cos \phi_{5R} \sin \theta_{\gamma_7} \sin \kappa) + \cos \beta \sin \theta_{\alpha_1} (\sin \phi_{5R} (\cos \kappa \cos \phi_{6R} \cos \theta_{\gamma_7} - \sin \theta_{\gamma_7} \sin \phi_{6R})) + \sin \beta \sin \theta_{\alpha_1} (\cos \kappa \cos \phi_{5R} - \sin \kappa \sin \phi_{5R} \cos \phi_{6R}) = 0, \tag{30}$$

$$\xi_{3R} := \sin \phi_{4R} (\cos \beta \sin \kappa \sin \phi_{6R} + \sin \beta (\sin \theta_{\gamma_7} \cos \phi_{6R} + \cos \theta_{\gamma_7} \sin \phi_{6R} \cos \kappa)) + \cos \phi_{4R} (\sin \beta (\cos \theta_{\gamma_7} \sin \kappa \sin \phi_{5R} - \cos \phi_{5R} (\cos \theta_{\gamma_7} \cos \kappa \cos \phi_{6R} - \sin \theta_{\gamma_7} \sin \phi_{6R})) - \cos \beta (\cos \phi_{5R} \cos \phi_{6R} \sin \kappa + \cos \kappa \sin \phi_{5R})) = 0. \tag{31}$$

It may be observed that Eqs. (26)–(31) are functions of the seven unknown variables appearing in the right chain, that is,  $\mathbf{q}_R = [\theta_{\alpha_1}, \theta_{2R}, \theta_{23R}, \phi_{4R}, \phi_{5R}, \phi_{6R}, \theta_{\gamma_7}]^T$ . From the elements of displacement vectors and rotation matrices of the left and right chains, that is, Eqs. (19)–(24) and Eqs. (26)–(31), equations with the least number of unknown variables appearing in them are chosen to construct the set of constraint equations defining the IKP. In this process, the IKP is defined in terms of the following constraint equations:  $\boldsymbol{\eta}_{IK} = \{\eta_1, \eta_2, \eta_3, \eta_4, \eta_5, \eta_6\} = \mathbf{0}$ . In the aforementioned equations,  $\{\eta_1, \eta_2, \eta_3, \eta_4, \eta_5, \eta_6\} = \{\eta_{1L}, \eta_{2L}, \eta_{3L}, \zeta_{1L}, \zeta_{2L}, \eta_{2R}\}$  (see Eqs. (19)–(23) and (27)) are functions of the unknown variables  $\mathbf{q} = [\theta_{\alpha_1}, \theta_{2L}, \theta_{23L}, \phi_{5L}, \psi_{6L}, \theta_{\gamma_7}]^T$ :

$$\eta_1(\theta_{\alpha_1}, \theta_{\gamma_7}, \psi_{6L}, \theta_{2L}, \theta_{23L}) = 0, \tag{32}$$

$$\eta_2(\theta_{\alpha_1}, \theta_{\gamma_7}, \psi_{6L}) = 0, \tag{33}$$

$$\eta_3(\theta_{\gamma_7}, \psi_{6L}, \theta_{2L}, \theta_{23L}) = 0, \tag{34}$$

$$\eta_4(\theta_{\alpha_1}, \theta_{\gamma_7}, \theta_{23L}, \phi_{5L}, \psi_{6L}) = 0, \tag{35}$$

$$\eta_5(\theta_{\gamma_7}, \theta_{23L}, \phi_{5L}, \psi_{6L}) = 0, \tag{36}$$

$$\eta_6(\theta_{\alpha_1}, \theta_{\gamma_7}) = 0. \tag{37}$$

In Eqs. (32)–(37), only the unknown variables are shown explicitly. The remaining six equations, that is, Eqs. (24), (26) and (28)–(31), are used later to solve for the remaining variables  $\{\phi_{4L}, \theta_{2R}, \theta_{23R}, \phi_{4R}, \phi_{5R}, \phi_{6R}\}$ . The order of elimination of variables is chosen based on the number of appearances, starting with the smallest one. In other words, the variable appearing in the lowest number of equations at each step is eliminated thereafter. This results in the following sequence of variables to be eliminated:  $\theta_{2L}, \phi_{5L}, \theta_{23L}, \psi_{6L}, \theta_{\gamma_7}$ . The details of these eliminations are presented in the following.

### 4.1. Elimination of $\theta_{2L}$

The constraint equations  $\eta_1 = 0$  (see (19)) and  $\eta_3 = 0$  (see (21)) are linear in the sine and cosine of  $\theta_{2L}$ , respectively. Hence, the expressions of  $\sin \theta_{2L}$  and  $\cos \theta_{2L}$  are obtained from Eqs. (19) and (21):

$$\sin \theta_{2L} = \frac{\lambda_1(\theta_{\alpha_1}, \theta_{\gamma_7}, \psi_{6L}, \theta_{23L})}{l_2}, \quad \cos \theta_{2L} = \frac{\lambda_2(\theta_{\gamma_7}, \psi_{6L}, \theta_{23L})}{l_2}, \quad \text{since } l_2 \neq 0. \tag{38}$$

In (38), the polynomials  $\lambda_1$  and  $\lambda_2$  are functions of the variables  $\theta_{\alpha_1}, \theta_{\gamma_7}, \psi_{6L}$  and  $\theta_{23L}$ . Substituting the expressions of  $\sin \theta_{2L}$  and  $\cos \theta_{2L}$  in the trigonometric identity  $\cos^2 \theta_{2L} + \sin^2 \theta_{2L} = 1$  leads to a new equation in the remaining variables, namely  $f(\theta_{\alpha_1}, \theta_{\gamma_7}, \psi_{6L}, \theta_{23L}) = 0$ . The resulting elimination of  $\theta_{2L}$  is depicted below schematically:<sup>10</sup>

$$\left. \begin{aligned} \eta_1(\theta_{\alpha_1}, \theta_{\gamma_7}, \psi_{6L}, \theta_{2L}, \theta_{23L}) = 0 \\ \eta_3(\theta_{\gamma_7}, \psi_{6L}, \theta_{2L}, \theta_{23L}) = 0 \end{aligned} \right\} \xrightarrow{\times \theta_{2L}} f(\theta_{\alpha_1}, \theta_{\gamma_7}, \psi_{6L}, \theta_{23L}) = 0. \tag{39}$$

### 4.2. Elimination of $\phi_{5L}$

Equations  $\eta_4 = 0$  and  $\eta_5 = 0$  (see Eqs. (22) and (23)) are linear in the sine and cosine of  $(\phi_{5L} + \psi_{6L})$  and hence may be represented as:

$$\eta_4 := i_1(\theta_{\alpha_1}) \cos(\phi_{5L} + \psi_{6L}) + j_1(\theta_{\alpha_1}, \theta_{\gamma_7}) \sin(\phi_{5L} + \psi_{6L}) + k_1(\theta_{23L}) = 0, \tag{40}$$

$$\eta_5 := i_2 \cos(\phi_{5L} + \psi_{6L}) + j_2(\theta_{\gamma_7}) \sin(\phi_{5L} + \psi_{6L}) + k_2(\theta_{23L}) = 0, \tag{41}$$

<sup>10</sup>In this paper, the symbol “ $\xrightarrow{\times x}$ ” implies the elimination of the variable  $x$  from two simultaneous equations in the variable  $x$ .

where the coefficients  $i_i, j_i$  and  $k_i$  are functions of the variables  $\theta_{23L}, \psi_{6L}$  and  $\theta_{\gamma}$ . The expressions of  $\sin(\phi_{5L} + \psi_{6L})$  and  $\cos(\phi_{5L} + \psi_{6L})$  are obtained from these equations and substituted in the trigonometric identity  $\cos^2(\phi_{5L} + \psi_{6L}) + \sin^2(\phi_{5L} + \psi_{6L}) = 1$  yielding:

$$n(\theta_{\alpha_1}, \theta_{\gamma}, \theta_{23L}) := \cos \theta_{23L} \sin \beta \sin \theta_{\gamma} - \sin \theta_{23L} (\cos \theta_{\gamma} \sin \theta_{\alpha_1} + \cos \beta \cos \theta_{\alpha_1} \sin \theta_{\gamma}) = 0. \tag{42}$$

The above equation is obtained assuming<sup>11</sup> that:

$$|ij| := (i_1 j_2 - i_2 j_1) \neq 0. \tag{43}$$

Equation (42) represents a kinematic constraint in the unknown variables  $\theta_{\alpha_1}, \theta_{\gamma}$ , and  $\theta_{23L}$ . Furthermore, the conditions  $i_1^2 + j_1^2 - k_1^2 = 0$  and  $i_2^2 + j_2^2 - k_2^2 = 0$  cause repeated roots to satisfy (40) and (41), respectively. The details of this singularity are discussed in Case 1 in Section 6.2.

### 4.3. Elimination of $\theta_{23L}$

The constraint equations  $n = 0$  (see (42)) and  $f = 0$  (see (39)) are both linear in the sine and cosine of  $\theta_{23L}$  and can be written explicitly in terms of  $\cos \theta_{23L}$  and  $\sin \theta_{23L}$  as:

$$n := a_1(\theta_{\gamma}) \cos \theta_{23L} + b_1(\theta_{\gamma}, \theta_{\alpha_1}) \sin \theta_{23L} = 0, \tag{44}$$

$$f := a_2(\theta_{\gamma}, \psi_{6L}) \cos \theta_{23L} + b_2(\theta_{\gamma}, \theta_{\alpha_1}, \psi_{6L}) \sin \theta_{23L} + c_2(\theta_{\gamma}, \theta_{\alpha_1}, \psi_{6L}) = 0. \tag{45}$$

As shown in Eqs. (44) and (45), the coefficients  $a_i, b_i$  and  $c_i$  ( $i = 1, 2$ ) are functions of the unknown variables  $\theta_{\alpha_1}, \psi_{6L}$  and  $\theta_{\gamma}$ . Subsequently, the variable  $\theta_{23L}$  is eliminated following the procedure described in Sections 4.1 and 4.2, leading to the equation:

$$h_1(\theta_{\gamma}, \theta_{\alpha_1}, \psi_{6L}) := c_2^2(a_1^2 + b_1^2) - |ab|^2 = 0. \tag{46}$$

It is assumed in the above that:

$$|ab| := (a_1 b_2 - a_2 b_1) \neq 0. \tag{47}$$

Transferring  $|ab|^2$  to the right-hand side of (46) and taking square roots of both the sides and rearranging, one obtains

$$h(\theta_{\gamma}, \theta_{\alpha_1}, \psi_{6L}) := c_2 \mu - |ab| = 0, \text{ where } \mu(\theta_{\gamma}, \theta_{\alpha_1}) := \pm \sqrt{a_1^2 + b_1^2}. \tag{48}$$

The size<sup>12</sup> of the symbolic expression of  $h$  is 13.080 KB.

The identification of the form of (46) was made possible solely by the exact symbolic approach adopted in this work. It has allowed the reduction of this equation to (48), a step which is of critical importance in the symbolic computation scheme leading to the final univariate equation. It is a key enabler in permitting the computation to continue in the exact symbolic form, for two reasons: (a) it halves the degrees of the relevant variables appearing in (46) and (b) it helps in reducing the sizes of the expressions involved rather dramatically, without which the subsequent computations would have been rendered impractical (due to the demands on computational resources and time) or even infeasible. Consider, for instance, (53), which is derived below after a few steps. If it were to be derived directly from (46), it would have had a size of 6.110 MB, which might have deterred subsequent symbolic computations. Also, the equation  $p = 0$  would have been a *quartic* in the variable  $c_6$ , making its elimination significantly more difficult in the computations that follow the derivation of (53). However, when the same equation is derived from (48), not only  $p$  becomes a *quadratic* function of  $c_6$ , as an expression, its

<sup>11</sup>It may be noted that in the case when  $i_1 j_2 - i_2 j_1 = 0$  (refer to (43)), Eqs. (40) and (41) become linearly dependent and the elimination procedure presented no longer holds true. This could occur due to the choice of the constraint equations and, therefore, does not necessarily lead to a singularity in the manipulator.

<sup>12</sup>In this article, the “size” of an expression refers to the amount of memory used internally by the CAS used in this work, namely *Mathematica* [31], to store and use the expression for performing symbolic computations. It is computed using the built-in command `ByteCount`.

size is reduced to only 19.232 KB, that is, it is reduced by a factor greater than 300. As mentioned in Section 7, this and similar custom-developed techniques in symbolic computation allow the derivation of the key results in this paper.

It may be noted from (44) that  $\theta_{23L}$  has finite number of values iff:

$$\mu \neq 0 \Rightarrow a_1^2 + b_1^2 \neq 0. \tag{49}$$

The condition  $|ab| = 0$  (see (47)), also caused<sup>13</sup> by  $\mu = 0$  (see (48)), results in a singularity of the manipulator. The details of the singularity are discussed in Case 2 in Section 6.2. Further, the condition  $a_2^2 + b_2^2 - c_2^2 = 0$  leads to a double root of (45). The corresponding singularity is also studied in Section 6.2, in Case 3. It is worth mentioning that a merger of the solutions of the variable  $\theta_{23L}$  leads to a repeated solution of the variable  $\theta_{2L}$  as well.

#### 4.4. Elimination of $\psi_{6L}$

The constraint equation  $\eta_2 = 0$  (see (20)) is linear in the cosine and sine of  $\psi_{6L}$  or, equivalently, linear in  $\{c_6, s_6\}$ , where  $c_6 = (a_6 - l_w \cos \psi_{6L})$  and  $s_6 = (d_7 - l_w \sin \psi_{6L})$ . Therefore, for the sake of convenience,  $\eta_2 = 0$  (see (20)) and  $h = 0$  (see (48)) are written in terms of  $\{c_6, s_6\}$  leading to the equations  $g_1(\theta_{\gamma_7}, \theta_{\alpha_1}, c_6, s_6) = 0$  and  $g_2(\theta_{\gamma_7}, \theta_{\alpha_1}, c_6, s_6) = 0$ , respectively:

$$\begin{aligned} \eta_2(\theta_{\gamma_7}, \theta_{\alpha_1}, \psi_{6L}) = 0 &\xrightarrow{\psi_{6L} \rightarrow c_6, s_6} g_1(\theta_{\gamma_7}, \theta_{\alpha_1}, c_6, s_6) = 0, \\ h(\theta_{\gamma_7}, \theta_{\alpha_1}, \psi_{6L}) = 0 &\xrightarrow{\psi_{6L} \rightarrow c_6, s_6} g_2(\theta_{\gamma_7}, \theta_{\alpha_1}, c_6, s_6) = 0. \end{aligned} \tag{50}$$

In the above, the symbol  $\xrightarrow{\psi_{6L} \rightarrow c_6, s_6}$  implies the absorption of the trigonometric variables of  $\psi_{6L}$  into the algebraic variables  $s_6$  and  $c_6$ . Subsequently, the expression of  $s_6$  is obtained in terms of  $c_6$  from  $g_1(\theta_{\gamma_7}, \theta_{\alpha_1}, c_6, s_6) = 0$ :<sup>14</sup>

$$s_6 = \frac{1}{\sin \beta \sin \theta_{\alpha_1}} \zeta(\theta_{\gamma_7}, \theta_{\alpha_1}, c_6), \text{ assuming } \sin \beta \sin \theta_{\alpha_1} \neq 0. \tag{51}$$

Substituting  $s_6$  from (51) in the modified trigonometric identity  $(a_6 - c_6)^2 + (d_7 - s_6)^2 = l_w^2$  yields a quadratic equation in  $c_6$ , denoted by  $g(\theta_{\gamma_7}, \theta_{\alpha_1}, c_6) = 0$ :

$$\left. \begin{aligned} g_1(\theta_{\gamma_7}, \theta_{\alpha_1}, c_6, s_6) = 0 \\ (a_6 - c_6)^2 + (d_7 - s_6)^2 - l_w^2 = 0 \end{aligned} \right) \xrightarrow{\times s_6} g(\theta_{\gamma_7}, \theta_{\alpha_1}, c_6) = 0. \tag{52}$$

Likewise, the expression of  $s_6$  presented in (51) is substituted in  $g_2 = 0$  (see (50)) to obtain a quadratic in  $c_6$  of size 19.232 KB, namely  $p(\theta_{\gamma_7}, \theta_{\alpha_1}, c_6) = 0$ :

$$\left. \begin{aligned} g_1(\theta_{\gamma_7}, \theta_{\alpha_1}, c_6, s_6) = 0 \\ g_2(\theta_{\gamma_7}, \theta_{\alpha_1}, c_6, s_6) = 0 \end{aligned} \right) \xrightarrow{\times s_6} p(\theta_{\gamma_7}, \theta_{\alpha_1}, c_6) = 0. \tag{53}$$

Hereafter, the equations  $g = 0$  and  $p = 0$  may be represented as:

$$g(\theta_{\gamma_7}, \theta_{\alpha_1}, c_6) := a_3 c_6^2 + b_3 c_6 + c_3 = 0, \tag{54}$$

$$p(\theta_{\gamma_7}, \theta_{\alpha_1}, c_6) := a_4 c_6^2 + b_4 c_6 + c_4 = 0, \tag{55}$$

<sup>13</sup>It is observed that  $c_2 = 0$  (see (48)) makes the Eqs. (44) and (45) linearly dependent. It is interesting to note that this could be attributed to the choice of the constraint equations and hence, the manipulator need not encounter a singularity if  $c_2 = 0$ .

<sup>14</sup>It is important to emphasise that when  $\sin \beta \sin \theta_{\alpha_1} = 0$  an alternative procedure involving the determination of  $c_6$  from  $g_1 = 0$  is to be pursued. The detailed process is not included for the sake of brevity. The obtained expression of  $c_6$  is then substituted in the modified trigonometric identity  $(a_6 - c_6)^2 + (d_7 - s_6)^2 - l_w^2 = 0$  and  $g_2 = 0$  to obtain the equations  $g = 0$  and  $p = 0$ , respectively. Subsequently, the resultant of  $g = 0$  and  $p = 0$  with respect to  $c_6$  yields  $q = 0$ . However, the singularity  $\mu = 0$  is encountered when both the coefficients of  $c_6$  and  $s_6$  are zero, the details of which are discussed in Case 2 of Section 6.2.

where the coefficients  $a_i, b_i$  and  $c_i$  ( $i = 3, 4$ ) are functions of the variables  $\theta_{\gamma_7}$  and  $\theta_{\alpha_1}$ . Simultaneous satisfaction of the conditions  $b_3^2 - 4a_3c_3 = 0$  and  $b_4^2 - 4a_4c_4 = 0$  causes the roots of Eqs. (54) and (55) to repeat. The corresponding singularity is discussed under Case 4 in Section 6.2. The resultant<sup>15</sup> of  $p = 0$  and  $g = 0$  with respect to  $c_6$  eliminates<sup>16</sup> the variable and leads to a new equation  $q(\theta_{\gamma_7}, \theta_{\alpha_1}) = 0$  of size 839.088 KB:

$$\begin{matrix} p(\theta_{\gamma_7}, \theta_{\alpha_1}, c_6) = 0 \\ g(\theta_{\gamma_7}, \theta_{\alpha_1}, c_6) = 0 \end{matrix} \xrightarrow{\times c_6} q(\theta_{\gamma_7}, \theta_{\alpha_1}) = 0. \tag{56}$$

As noted before, the elimination of  $c_6$  was greatly facilitated by the reduction of (46) to (48). Continuing further, the function  $q = 0$  was simplified symbolically,<sup>17</sup> which afforded its factorisation in the following manner:

$$q(\theta_{\gamma_7}, \theta_{\alpha_1}) := \mu^3 \sin^2 \beta \sin^2 \theta_{\alpha_1} \delta(\theta_{\gamma_7}, \theta_{\alpha_1}) = 0, \tag{57}$$

where  $\delta(\theta_{\gamma_7}, \theta_{\alpha_1})$  is a cubic polynomial in  $\mu$ . Since it has already been assumed that  $\mu \neq 0$  and  $\sin \beta \sin \theta_{\alpha_1} \neq 0$  (in the context of Eqs. (49) and (51)), (57) reduces to  $\delta(\theta_{\gamma_7}, \theta_{\alpha_1}) = 0$ , which may be written as:

$$\delta(\theta_{\gamma_7}, \theta_{\alpha_1}) := m_0\mu^3 + m_1\mu^2 + m_2\mu + m_3 = 0. \tag{58}$$

The coefficients in (58), namely  $m_i$ , are also functions of the variables  $\theta_{\gamma_7}$  and  $\theta_{\alpha_1}$ . Since it is known (from (48)) that  $\mu^2 = a_1^2 + b_1^2$ , (58) is manipulated to derive its equivalent, cast in terms of  $\mu^2$ :

$$\delta_1(\theta_{\gamma_7}, \theta_{\alpha_1}) := (m_0\mu^2 + m_2)^2\mu^2 - (m_1\mu^2 + m_3)^2 = 0. \tag{59}$$

Direct substitution of the expressions of the coefficients  $m_i$  and  $\mu^2$  in (59) leads to the following equation free of radicals:

$$\begin{matrix} \delta_1(\theta_{\gamma_7}, \theta_{\alpha_1}) = 0 \\ \mu^2 - (a_1^2 + b_1^2) = 0 \end{matrix} \xrightarrow{\times \mu^2} r(\theta_{\gamma_7}, \theta_{\alpha_1}) = 0. \tag{60}$$

However, the size of  $r(\theta_{\gamma_7}, \theta_{\alpha_1})$ , even after rigorous simplification, stands at 216.140 MB. It is reduced in the next step, before proceeding further.

#### 4.5. Elimination of $\theta_{\gamma_7}$

The expression  $r(\theta_{\gamma_7}, \theta_{\alpha_1})$  turns out to be cubic in  $\cos \theta_{\gamma_7}$ . However, using the identities:

$$\cos^{2m} \theta_{\alpha_1} = (1 - \sin^2 \theta_{\alpha_1})^m, \quad m \in \mathbb{Z}^+, \tag{61}$$

(60) is reduced to:

$$r_l(\theta_{\gamma_7}, \theta_{\alpha_1}) = 0. \tag{62}$$

<sup>15</sup>All the resultants computed in this paper employed the built-in function `Resultant` of the CAS `Mathematica` [31].

<sup>16</sup>It may be noted that when  $a_3b_4 - b_3a_4$  vanishes, Eqs. (54) and (55) become linearly dependent and the procedure of elimination fails. This is typically a mathematical artefact of the computation scheme, and as such, it does not necessarily imply a physical singularity of the actual manipulator.

<sup>17</sup>All symbolic simplifications mentioned in this paper were performed using the customised schemes introduced in Section 3 of [24], the details of which are omitted for the want of space.

The polynomial  $r_l$  is linear in  $\cos \theta_{\gamma}$ . Furthermore, this reduction results in fewer coefficients, which, upon symbolic simplification, shrink to the size of 89.311 MB. It may be noted here that the equation  $\eta_6 = 0$  (see (27)), is also linear in  $\cos \theta_{\gamma}$  and  $\sin \theta_{\gamma}$ , from which one can find  $\cos \theta_{\gamma}$  in terms of  $\sin \theta_{\gamma}$ .<sup>18</sup>

$$\cos \theta_{\gamma} = \frac{v(\theta_{\alpha_1}, \sin \theta_{\gamma})}{(a_6 - l_w \cos \kappa) \cos \beta \sin \theta_{\alpha_1}}, \text{ assuming } (a_6 - l_w \cos \kappa) \cos \beta \sin \theta_{\alpha_1} \neq 0. \tag{63}$$

In (63),  $v(\theta_{\alpha_1}, \sin \theta_{\gamma})$  is linear in  $\cos \theta_{\alpha_1}$ ,  $\sin \theta_{\alpha_1}$  and  $\sin \theta_{\gamma}$ . Substituting the expression of  $\cos \theta_{\gamma}$  in (62) results in a sextic equation in  $\sin \theta_{\gamma}$ , namely  $u_1(\theta_{\alpha_1}, \sin \theta_{\gamma}) = 0$ :

$$\left. \begin{aligned} \eta_6(\theta_{\gamma}, \theta_{\alpha_1}) = 0 \\ r_l(\theta_{\gamma}, \theta_{\alpha_1}) = 0 \end{aligned} \right) \xrightarrow{\times \cos \theta_{\gamma}} u_1(\theta_{\alpha_1}, \sin \theta_{\gamma}) = 0. \tag{64}$$

It may be noted here that the reduction of (60) to (62) is yet another improvisation in symbolic computation which has played a crucial role in the derivation of the inverse kinematic univariate (IKU) in its symbolic form. Specifically, if the equation  $r = 0$  was used in (64) instead of  $r_l = 0$ , the resulting size of  $u_1$  would have been 191.635 MB. However, due to the said reduction, the actual size turns out to be 79.873 MB, which allows the computation to proceed further.

In the next step, the expression of  $\cos \theta_{\gamma}$  (from (63)) is substituted in the trigonometric identity  $\cos^2 \theta_{\gamma} + \sin^2 \theta_{\gamma} = 1$ , to obtain a quadratic equation in  $\sin \theta_{\gamma}$ , namely  $u_2(\theta_{\alpha_1}, \sin \theta_{\gamma}) = 0$ :

$$\left. \begin{aligned} \eta_6(\theta_{\gamma}, \theta_{\alpha_1}) = 0 \\ \cos^2 \theta_{\gamma} + \sin^2 \theta_{\gamma} - 1 = 0 \end{aligned} \right) \xrightarrow{\times \cos \theta_{\gamma}} u_2(\theta_{\alpha_1}, \sin \theta_{\gamma}) = 0. \tag{65}$$

Eliminating  $\sin \theta_{\gamma}$  between Eqs. (64) and (65) yields the univariate equation in  $\theta_{\alpha_1}$ , that is,  $u(\theta_{\alpha_1}) = 0$ , which is of total degree 26 in  $\sin \theta_{\alpha_1}$  and  $\cos \theta_{\alpha_1}$ :

$$\left. \begin{aligned} u_1(\theta_{\alpha_1}, \sin \theta_{\gamma}) = 0 \\ u_2(\theta_{\alpha_1}, \sin \theta_{\gamma}) = 0 \end{aligned} \right) \xrightarrow{\times \sin \theta_{\gamma}} u(\theta_{\alpha_1}) = 0. \tag{66}$$

Therefore, one may arrive at the final univariate polynomial from (66), as described in the next subsection. However, before that, a few special cases must be considered, for the sake of completeness.

It may be noted that repeated roots in the sextic equation  $u_1 = 0$  (see (64)) and the quadratic equation  $u_2 = 0$  (see (65)) cause the manipulator to encounter a singularity. The sextic  $u_1 = 0$  (see (64)) is a polynomial equation in  $s_7 = \sin \theta_{\gamma}$  and its discriminant may be obtained as:

$$\Delta_1 = \text{res} \left( u_1, \frac{\partial u_1}{\partial s_7}, s_7 \right). \tag{67}$$

In (67),  $\text{res}(a(x), b(x), x)$  denotes the resultant of the polynomials  $a(x)$  and  $b(x)$  w.r.t.  $x$ . Further, Equation (65) may be written as:

$$u_2(\theta_{\alpha_1}, \sin \theta_{\gamma}) := a_5 \sin^2 \theta_{\gamma} + b_5 \sin \theta_{\gamma} + c_5 = 0. \tag{68}$$

In (68), the coefficients  $a_5$ ,  $b_5$  and  $c_5$  are functions of  $\theta_{\alpha_1}$  alone. Hence, the manipulator encounters a singularity when the discriminants of Eqs. (64) and (65), that is,  $\Delta_1$  (see (67)) and  $b_5^2 - 4a_5c_5$  (see (68)), respectively, vanish simultaneously. The corresponding singularity is studied as Case 5 in Section 6.2.

<sup>18</sup>It is worth mentioning that if  $\cos \beta \sin \theta_{\alpha_1} = 0$  (the term  $(a_6 - l_w \cos \kappa)$  cannot vanish for the values of architecture parameters chosen in this article (see Table III)) an alternative procedure requiring the calculation of  $\sin \theta_{\gamma}$  from (27) is to be pursued. The process, being very similar to the one used above, is explained very briefly for the sake of completeness. The expression of  $\sin \theta_{\gamma}$  is substituted in  $r_l = 0$  and the trigonometric identity  $\cos^2 \theta_{\gamma} + \sin^2 \theta_{\gamma} - 1 = 0$  to yield equations  $u_1 = 0$  and  $u_2 = 0$ , respectively. Thereafter, the resultant of  $u_1 = 0$  and  $u_2 = 0$  with respect to  $\cos \theta_{\gamma}$  results in  $u = 0$ . However, when both the coefficients of  $\cos \theta_{\gamma}$  and  $\sin \theta_{\gamma}$  vanish, that is,  $\cos^2 \theta_{\alpha_1} + \cos^2 \beta \sin^2 \theta_{\alpha_1} = 0$ , a singularity is encountered, as discussed in Case 1 in Section 6.2.

**Table III.** Values of the architecture parameters (see Fig. 1) of the manipulator used for the numerical examples.

| Parameter | $d_2$         | $l_2$ | $l_3$             | $l_w$ | $\kappa$         | $a_6$         | $d_7$         |
|-----------|---------------|-------|-------------------|-------|------------------|---------------|---------------|
| Value     | $\frac{1}{2}$ | 3     | $\frac{269}{100}$ | 1     | $\frac{2\pi}{3}$ | $\frac{1}{2}$ | $\frac{1}{2}$ |

**4.6. Derivation of the IKU equation**

In the following, the total degree of the equation  $u = 0$  (66) in  $\sin \theta_{\alpha_1}$  and  $\cos \theta_{\alpha_1}$  is brought down from 26 to 20 through the identification and subsequent rejection of *spurious factors*, which are associated with singular solutions. Once again, this is an important step involving symbolic simplification and factorisation, without which the final univariate polynomial equation, that is, the IKU, would have been of degree 52, and not 40, as it is in (74).

The elimination process in (66) is simplified by rewriting  $u_1 = 0$  and  $u_2 = 0$  as polynomial equations in  $\sin \theta_{\gamma_7}$ :

$$u_1 := \tau(\theta_{\alpha_1})u_{16} \sin^6 \theta_{\gamma_7} + u_{15} \sin^5 \theta_{\gamma_7} + u_{14} \sin^4 \theta_{\gamma_7} + u_{13} \sin^3 \theta_{\gamma_7} + u_{12} \sin^2 \theta_{\gamma_7} + u_{11} \sin \theta_{\gamma_7} + u_{10} = 0, \tag{69}$$

$$u_2 := \tau(\theta_{\alpha_1}) \sin^2 \theta_{\gamma_7} + u_{21} \sin \theta_{\gamma_7} + u_{20} = 0. \tag{70}$$

In the preceding equations, the coefficients  $u_{ij}$  are functions of  $\theta_{\alpha_1}$ ; also,

$$\tau(\theta_{\alpha_1}) := \cos^2 \theta_{\alpha_1} + \cos^2 \beta \sin^2 \theta_{\alpha_1}. \tag{71}$$

Thus, the resulting equation  $u(\theta_{\alpha_1}) = 0$  obtained by the elimination of  $\sin \theta_{\gamma_7}$  from Eqs. (69) and (70) depends on  $u_{ij}(\theta_{\alpha_1})$  and  $\tau(\theta_{\alpha_1})$ , that is, ultimately, on  $\theta_{\alpha_1}$  alone. It is interesting to note that  $\tau(\theta_{\alpha_1}) = 0$  trivially satisfies (70) and therefore,  $\tau(\theta_{\alpha_1}) \neq 0$  for  $\theta_{\gamma_7}$  to have finite number of values. Expressing  $u(\theta_{\alpha_1}) = 0$  in terms of the coefficients  $u_{ij}$  affords the advantage of yielding the factor  $\tau^2(\theta_{\alpha_1})$  without having to handle the large-sized expressions of  $u_{ij}$ :

$$u(\theta_{\alpha_1}) := \tau^2(\theta_{\alpha_1})w_1(\theta_{\alpha_1}) = 0, \tag{72}$$

where  $w_1(\theta_{\alpha_1})$  is a function of  $u_{ij}$ . As the factor  $\tau(\theta_{\alpha_1})$  appears in the leading coefficients of Eqs. (69) and (70), the manipulator encounters a singularity when  $\tau(\theta_{\alpha_1}) = 0$ , which is described in Case 1 of Section 6.2. Therefore, in the non-singular cases, the relevant part of (72) is given by  $w_1(\theta_{\alpha_1}) = 0$ . Subsequently, the actual expressions of the variables  $u_{ij}$  are substituted in  $w_1 = 0$ , along with the architecture parameters mentioned in Table III, which increases the size of  $w_1 = 0$  significantly to 25.388 MB even before its symbolic expansion, making further computation time-consuming and computationally complex. To overcome the aforementioned issues, the coefficients  $u_{ij}$  are transformed to the respective *monomial-based canonical* (MBC) forms (see ref. [24], Section 3, for the details), treating  $\sin \theta_{\gamma_7}$  and  $\cos \theta_{\gamma_7}$  as algebraic variables. Consequently, substituting these expressions of the coefficients  $u_{ij}$  in  $w_1 = 0$  results in  $w_2(\sin \theta_{\alpha_1}, \cos \theta_{\alpha_1}) = 0$ , which is a polynomial of total degree 22 in  $\sin \theta_{\alpha_1}$  and  $\cos \theta_{\alpha_1}$ . The maximum degrees of  $\cos \theta_{\alpha_1}$  and  $\sin \theta_{\alpha_1}$  in  $w_2(\theta_{\alpha_1})$  are 4 and 22, respectively. Subsequently,  $w_2$  is reduced to a linear function of  $\cos \theta_{\alpha_1}$  using the identities mentioned in (61), which is represented as  $w_s(\sin \theta_{\alpha_1}, \cos \theta_{\alpha_1}) = 0$ . Furthermore, the coefficients of each term of the form  $\sin^{n_s} \theta_{\alpha_1} \cos^{n_c} \theta_{\alpha_1}$ , where  $n_s, n_c \in \mathbb{N}$ , are isolated and simplified individually (due to the use of the MBC form), which reveals that the coefficients of the following terms vanish identically:  $\sin \theta_{\alpha_1}$ ,  $\cos \theta_{\alpha_1}$  and  $\cos \theta_{\alpha_1} \sin \theta_{\alpha_1}$ , and so does the constant term (i.e., the term corresponding to  $n_c = n_s = 0$ ). Once again, identification of such structural properties of the polynomial has been made possible only due to the application of specialised symbolic simplification routines, and it leads to a factorisation of  $w_s = 0$  in the following manner, which

was otherwise intractable using the default routines provided by the CAS due to extreme complexity of the computations involved:

$$w_s(\theta_{\alpha_1}) := \sin^2 \theta_{\alpha_1} \xi(\theta_{\alpha_1}) = 0. \tag{73}$$

In (73),  $\xi(\theta_{\alpha_1})$  is a polynomial of total degree 20 in  $\sin \theta_{\gamma_7}$  and  $\cos \theta_{\gamma_7}$ . Moreover, (73) reduces to  $\xi(\theta_{\alpha_1}) = 0$  as  $\sin \theta_{\alpha_1} \neq 0$ , as explained in the context of (63). Subsequently, the equation  $\xi = 0$  is converted to its algebraic form, in terms of  $t_1 = \tan(\theta_{\alpha_1}/2)$ , to obtain an IKU of degree 40,  $v(t_1) = 0$ , in the new unknown  $t_1$ :

$$v(t_1) := \vartheta_0 t_1^{40} + \vartheta_1 t_1^{39} + \vartheta_2 t_1^{38} + \dots + \vartheta_{38} t_1^2 + \vartheta_{39} t_1 + \vartheta_{40} = 0. \tag{74}$$

It may be appreciated at this point that without the detailed multi-step and specialised symbolic manipulations and simplifications, the explicit understanding of the structure of the polynomial equations involved and their factorisations would not have been possible. Consequently, one would have obtained an IKU of degree 52, as noted before. Because of all the steps mentioned above, the final polynomial equation has been obtained in its *minimal degree*, without any spurious roots.<sup>19</sup> Furthermore, in (74), the coefficients  $\vartheta_i$  are explicit symbolic functions of the task-space coordinates, which ensures that the nature of the analysis is generic over the entire task space. Consequently, the expressions of the coefficients are huge in their sizes,<sup>20</sup> as listed below (in GBs), starting from that of  $\vartheta_0$ , running through to  $\vartheta_{40}$ :

$$\{0.872, 1.691, 4.228, 7.515, 13.393, 20.658, 30.779, 41.951, 55.085, 67.850, 80.946, 91.987, 102.013, 109.060, 114.839, 117.865, 120.333, 120.874, 121.749, 121.380, 70.737, 121.380, 121.749, 120.874, 120.333, 117.865, 114.839, 109.060, 102.013, 91.987, 80.946, 67.850, 55.085, 41.951, 30.779, 20.658, 13.393, 7.515, 4.228, 1.691, 0.872\}. \tag{75}$$

The above-mentioned large-sized expressions could only be manipulated by expressing them as polynomials in the *nested canonical form* (see ref. [24], Section 3, for the details) in the position coordinates of the end-effector,  $\mathbf{p}$ , such that each of their coefficients reduced to only a few kilobytes in size and is solely in terms of the trigonometric functions of the Euler angles expressing the orientation of the end-effector frame. This improvisation not only reduces the computational complexity involved in simplification but also leads to significant reduction in sizes of the subsequent expressions.

The IKU equation is derived and solved in the context of a numerical example in Section 5.2, and the results are presented in Table VI and Fig. 4. Furthermore, due to the symbolic nature of the IKU, its *discriminant*,  $\Delta_2$ , may be computed as below, the vanishing of which is the condition for a repeated root of the IKU, implying a singularity.

$$\Delta_2 = \text{res} \left( v, \frac{\partial v}{\partial t_1}, t_1 \right). \tag{76}$$

The corresponding singularity is discussed in Case 6 of Section 6.2.

With the knowledge of 40 solutions of  $\theta_{\alpha_1}$  from the solution of the IKU equation, the corresponding solutions of  $\theta_{\gamma_7}$ ,  $\psi_{6L}$ ,  $\theta_{23L}$ ,  $\phi_{5L}$  and  $\theta_{2L}$  are obtained from Eqs. (37) and (60), Eqs. (33), (46), and (47), Eqs. (22), (23) and (38), respectively, leading to a set of 40 solutions of the variables  $\{\theta_{\alpha_1}, \theta_{\gamma_7}, \psi_{6L}, \theta_{23L}, \phi_{5L}, \theta_{2L}\}$ .

<sup>19</sup>It has been checked independently in the *numerical algebraic geometry* tool Bertini [32] that there are 40 branches of (finite) solutions in the complex plane to the IKP, which corroborates with the findings of this paper and supports the claim of minimality of the derived IKU.

<sup>20</sup>The computations corresponding to obtaining the coefficients of the IKU as functions of task-space coordinates have been performed on a server with 256 GB RAM and AMD® Opteron™ 6376 running at 2.3 GHz clock speed.

**Table IV.** Forward kinematics solutions for  $\theta_1 = \frac{\pi}{10}$ ,  $\theta_{2L} = \frac{\pi}{3}$ ,  $\theta_{3L} = \frac{\pi}{6}$ ,  $\theta_{2R} = \frac{\pi}{6}$ ,  $\theta_{3R} = \frac{\pi}{3}$  and  $\theta_7 = \frac{\pi}{4}$ , the corresponding poses of which are displayed in Fig. 2.

| Branch   | $\phi_{4L}$     | $\phi_{5L}$     | $\phi_{6L}$    | $\phi_{4R}$     | $\phi_{5R}$     | $\phi_{6R}$    | $p_x$          | $p_y$          | $p_z$          | $\alpha$       | $\beta$        | $\gamma$        | $e_{FK} (\times 10^{-16})$ |
|----------|-----------------|-----------------|----------------|-----------------|-----------------|----------------|----------------|----------------|----------------|----------------|----------------|-----------------|----------------------------|
| <b>1</b> | <b>-0.83211</b> | <b>-0.24301</b> | <b>2.35431</b> | <b>-0.83211</b> | <b>2.11130</b>  | <b>0</b>       | <b>5.17431</b> | <b>1.03851</b> | <b>2.72026</b> | <b>1.19556</b> | <b>2.27373</b> | <b>-1.27501</b> | <b>1.11022</b>             |
| 2        | 2.30948         | -2.11130        | 2.35431        | 2.30948         | 0.24301         | 0              | 3.48671        | 1.28818        | 1.89027        | 0.92429        | 2.13239        | 1.70523         | 0.62063                    |
| 3        | -0.83211        | -1.03030        | -2.35431       | -0.83211        | 2.89858         | 0              | 4.82610        | 1.48742        | 2.13329        | 2.28938        | 2.36092        | -0.49020        | 0.62063                    |
| 4        | 2.30948         | 3.38460         | -2.35431       | 2.30948         | 1.03030         | 0              | 4.26210        | 1.57135        | 1.85425        | 0.32554        | 1.58329        | 1.52416         | 1.11022                    |
| <b>5</b> | <b>-0.83211</b> | <b>-0.24301</b> | <b>2.35431</b> | <b>2.30948</b>  | <b>-2.11130</b> | <b>3.14159</b> | <b>5.17431</b> | <b>1.03851</b> | <b>2.72026</b> | <b>1.19556</b> | <b>2.27373</b> | <b>-1.27501</b> | <b>1.11022</b>             |
| 6        | 2.30948         | -2.11130        | 2.35431        | -0.83211        | -0.24301        | 3.14159        | 3.48671        | 1.28818        | 1.89027        | 0.92429        | 2.13239        | 1.70523         | 0.62063                    |
| 7        | -0.83211        | -1.03030        | -2.35431       | 2.30948         | -2.89858        | 3.14159        | 4.82610        | 1.48742        | 2.13329        | 2.28938        | 2.36092        | -0.49020        | 0.62063                    |
| 8        | 2.30948         | 3.38460         | -2.35431       | -0.83211        | -1.03030        | 3.14159        | 4.26210        | 1.57135        | 1.85425        | 0.32554        | 1.58329        | 1.52416         | 1.11022                    |

**Table V.** Monic form of the IKU in (74) for  $\alpha = 1.19556$ ,  $\beta = 2.27373$ ,  $\gamma = -1.27501$ ,  $p_x = 5.17431$ ,  $p_y = 1.03851$  and  $p_z = 2.72026$ .

| Coefficient  | Term     | Coefficient    | Term     | Coefficient    | Term     | Coefficient   | Term  |
|--------------|----------|----------------|----------|----------------|----------|---------------|-------|
| 12.23931     | $t^{39}$ | -5494.26626    | $t^{29}$ | -1874022.90191 | $t^{19}$ | -28,861.44935 | $t^9$ |
| 66.27187     | $t^{38}$ | -313847.64900  | $t^{28}$ | 325810.99841   | $t^{18}$ | -6922.19929   | $t^8$ |
| 200.50021    | $t^{37}$ | -290216.59880  | $t^{27}$ | 1330215.97448  | $t^{17}$ | 9796.91903    | $t^7$ |
| 282.39213    | $t^{36}$ | 532500.99114   | $t^{26}$ | -431064.77342  | $t^{16}$ | -2890.36845   | $t^6$ |
| -469.31658   | $t^{35}$ | 921007.08077   | $t^{25}$ | -676029.67510  | $t^{15}$ | -513.66449    | $t^5$ |
| -3795.72323  | $t^{34}$ | -541401.12877  | $t^{24}$ | 388719.92885   | $t^{14}$ | 720.26687     | $t^4$ |
| -9333.32596  | $t^{33}$ | -1627476.72169 | $t^{23}$ | 198961.53564   | $t^{13}$ | -281.97621    | $t^3$ |
| -3736.82898  | $t^{32}$ | 364320.84149   | $t^{22}$ | -221421.39467  | $t^{12}$ | 60.74087      | $t^2$ |
| 40,005.59585 | $t^{31}$ | 2009887.81427  | $t^{21}$ | 3353.56737     | $t^{11}$ | -7.28261      | $t^1$ |
| 94,474.52047 | $t^{30}$ | -252378.62487  | $t^{20}$ | 71,247.08879   | $t^{10}$ | 0.38293       | $t^0$ |

**4.7. Calculation of the remaining unknown variables**

In the following, a procedure for obtaining the variables which remain unknown till this point, that is,  $\theta_{2R}$ ,  $\theta_{23R}$ ,  $\phi_{4L}$ ,  $\phi_{4R}$ ,  $\phi_{5R}$ , and  $\phi_{6R}$ , is explained.

Equations (26) and (28) are linear in the sine and cosine of the angles  $\theta_{2R}$  and  $\theta_{23R}$ . Hence, the expressions of  $\cos \theta_{23R}$  and  $\sin \theta_{23R}$  are calculated from Eqs. (26) and (28), respectively:

$$\cos \theta_{23R} = \frac{\varepsilon_1(\theta_{\gamma}, \theta_{2R})}{l_3}, \quad \sin \theta_{23R} = \frac{\varepsilon_2(\theta_{\alpha_1}, \theta_{\gamma}, \theta_{2R})}{l_3}, \text{ since } l_3 \neq 0, \text{ and}$$

$$\varepsilon_1(\theta_{\gamma}, \theta_{2R}) := p_z + (d_7 - l_w \sin \kappa) \cos \beta + (a_6 - l_w \cos \kappa) \sin \beta \cos \theta_{\gamma} - l_2 \cos \theta_{2R}, \tag{77}$$

$$\varepsilon_2(\theta_{\alpha_1}, \theta_{\gamma}, \theta_{2R}) := p_x \cos(\alpha - \theta_{\alpha_1}) + p_y \sin(\alpha - \theta_{\alpha_1}) + (d_7 - l_w \sin \kappa) \cos \theta_{\alpha_1} \sin \beta + (a_6 - l_w \cos \kappa)(\sin \theta_{\alpha_1} \sin \theta_{\gamma} - \cos \beta \cos \theta_{\alpha_1} \cos \theta_{\gamma}). \tag{78}$$

Thereafter, substituting the expressions of  $\cos \theta_{23R}$  and  $\sin \theta_{23R}$  from (77) in the identity  $\cos^2 \theta_{23R} + \sin^2 \theta_{23R} = 1$  results in equation  $o(\theta_{\alpha_1}, \theta_{\gamma}, \theta_{2R}) = 0$ :

$$o(\theta_{\alpha_1}, \theta_{\gamma}, \theta_{2R}) := o_1(\theta_{\gamma}) \cos \theta_{2R} + o_2(\theta_{\alpha_1}, \theta_{\gamma}) \sin \theta_{2R} + o_3(\theta_{\gamma}) = 0. \tag{79}$$

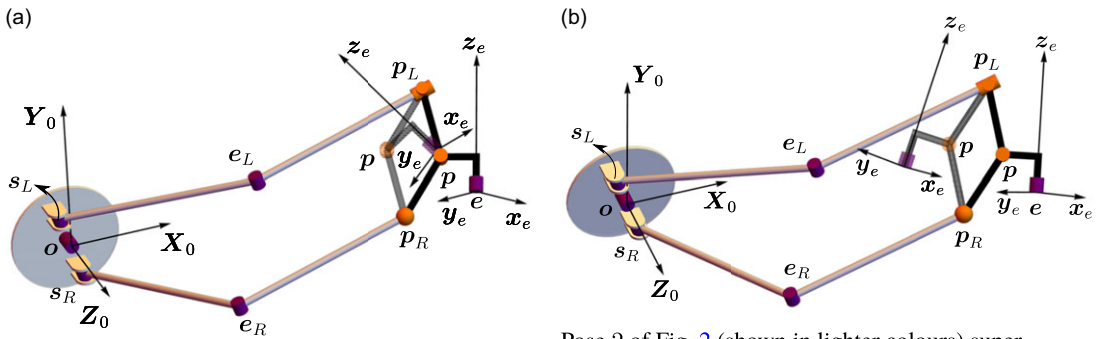
In (79), the coefficients  $o_i$  are functions of  $\theta_{\alpha_1}$  and  $\theta_{\gamma}$ . Subsequently, the equation is solved for known values of  $\theta_{\alpha_1}$  and  $\theta_{\gamma}$ , resulting in 80 solutions of the variables  $\{\theta_{\alpha_1}, \theta_{\gamma}, \psi_{6L}, \theta_{23L}, \phi_{5L}, \theta_{2L}, \theta_{23R}, \theta_{2R}\}$ , in the general case. It may be noticed that a singularity is encountered when  $o_1^2 + o_2^2 - o_3^2$  vanishes, as the solutions of the variables  $\theta_{2R}$  and  $\theta_{23R}$  merge in this condition. This is discussed in detail in Section 6.2, in Case 7.

The remaining passive joint variables, namely  $\phi_{4L}$ ,  $\phi_{4R}$ ,  $\phi_{5R}$  and  $\phi_{6R}$  may be obtained using Eqs. (11), (14)–(16), for the known values of the active joint angles and the passive joint angles  $\phi_{5L}$ ,  $\phi_{6L}$ . Since the solution procedure for calculating the passive joint variables for the known active joint angles has previously been covered as part of the FKP in Section 3, the corresponding details are not presented here again for the sake of brevity. While the variable  $\phi_{4L}$  has a unique solution, the variables  $\phi_{4R}$ ,  $\phi_{5R}$  and  $\phi_{6R}$  have two sets of solutions. Thus, in total, the IKP leads to a total of 160 solutions (including complex ones) for a generic pose of the end-effector in  $\mathbb{SE}(3)$ .

It may be noted, however, that even though the total number of solutions is rather high at 160, the actual physical situation is not really as complex. There are only 40 main/independent branches of solutions, which is not uncharacteristically high in the domain of kinematics, as the general 6-6-Stewart platform manipulator has the same number of solutions for its FKP [25], and the SNU 3-UPU has 78 solutions to its FKP [26]. Within each of these 40 main branches, four sub-branches appear, two of which essentially correspond to the *elbow-up* and *elbow-down* configurations of the right 2-R arm at the elbow joint  $e_R$ . It is interesting that the other two sub-branches, which are attributed to the spherical joint at  $p_R$ ,

**Table VI.** Inverse kinematics solutions for  $\alpha = 1.19556$ ,  $\beta = 2.27373$ ,  $\gamma = -1.27501$ ,  $p_x = 5.17431$ ,  $p_y = 1.03851$  and  $p_z = 2.72026$ , the corresponding poses of which are displayed in Fig. 4.

| Branch    | $\theta_1$     | $\theta_{2L}$  | $\theta_{3L}$  | $\theta_{2R}$  | $\theta_{3R}$  | $\theta_7$     | $\phi_{4L}$     | $\phi_{5L}$     | $\phi_{6L}$     | $\phi_{4R}$     | $\phi_{5R}$     | $\phi_{6R}$     | $e_{IK} (\times 10^{-6})$ |
|-----------|----------------|----------------|----------------|----------------|----------------|----------------|-----------------|-----------------|-----------------|-----------------|-----------------|-----------------|---------------------------|
| 1         | 0.23523        | 1.78022        | -0.95775       | 0.57762        | 1.05418        | 1.21708        | -0.88969        | 0.83837         | -4.38393        | -1.29552        | 1.99699         | -0.52421        | 5.50971                   |
| 2         | 0.23523        | 1.78022        | -0.95775       | 0.57762        | 1.05418        | 1.21708        | -0.88969        | 0.83837         | -4.38393        | 1.84607         | -1.99699        | 2.61738         | 5.50971                   |
| 3         | 0.23523        | 1.78022        | -0.95775       | 1.56841        | -1.05418       | 1.21708        | -0.88969        | 0.83837         | -4.38393        | -0.04847        | 2.89120         | 0.88031         | 5.50971                   |
| 4         | 0.23523        | 1.78022        | -0.95775       | 1.56841        | -1.05418       | 1.21708        | -0.88969        | 0.83837         | -4.38393        | 3.09312         | -2.89120        | -2.26128        | 5.50971                   |
| 5         | 0.30984        | 1.08507        | 0.44881        | 0.52456        | 1.05176        | 0.80977        | -0.84354        | -0.26981        | -3.87174        | -0.86086        | 2.10968         | -0.03287        | 5.34075                   |
| 6         | 0.30984        | 1.08507        | 0.44881        | 0.52456        | 1.05176        | 0.80977        | -0.84354        | -0.26981        | -3.87174        | 2.28073         | -2.10968        | 3.10872         | 5.34075                   |
| 7         | 0.30984        | 1.08507        | 0.44881        | 1.51310        | -1.05176       | 0.80977        | -0.84354        | -0.26981        | -3.87174        | 0.30196         | 2.51557         | 1.48951         | 5.34075                   |
| 8         | 0.30984        | 1.08507        | 0.44881        | 1.51310        | -1.05176       | 0.80977        | -0.84354        | -0.26981        | -3.87174        | -2.83963        | -2.51557        | -1.65208        | 5.34075                   |
| <b>9</b>  | <b>0.31416</b> | <b>1.04721</b> | <b>0.52357</b> | <b>0.52360</b> | <b>1.04720</b> | <b>0.78541</b> | <b>-0.83211</b> | <b>-0.24302</b> | <b>-3.92885</b> | <b>-0.83212</b> | <b>2.11130</b>  | <b>-0.00001</b> | <b>5.32751</b>            |
| <b>10</b> | <b>0.31416</b> | <b>1.04721</b> | <b>0.52357</b> | <b>0.52360</b> | <b>1.04720</b> | <b>0.78541</b> | <b>-0.83211</b> | <b>-0.24302</b> | <b>-3.92885</b> | <b>2.30947</b>  | <b>-2.11130</b> | <b>3.14158</b>  | <b>5.32751</b>            |
| 11        | 0.31416        | 1.04721        | 0.52357        | 1.50791        | -1.04720       | 0.78541        | -0.83211        | -0.24302        | -3.92885        | 0.30076         | 2.49250         | 1.50386         | 5.32751                   |
| 12        | 0.31416        | 1.04721        | 0.52357        | 1.50791        | -1.04720       | 0.78541        | -0.83211        | -0.24302        | -3.92885        | -2.84084        | -2.49250        | -1.6377         | 5.32751                   |
| 13        | 0.33645        | 0.79789        | 0.95181        | 0.52315        | 1.01417        | 0.65487        | -0.75849        | 0.13405         | -4.44948        | -0.67751        | 2.10789         | 0.179027        | 4.78108                   |
| 14        | 0.33645        | 0.79789        | 0.95181        | 0.52315        | 1.01417        | 0.65487        | -0.75849        | 0.13405         | -4.44948        | 2.46408         | -2.10789        | -2.96257        | 4.78108                   |
| 15        | 0.33645        | 0.79789        | 0.95181        | 1.47681        | -1.01417       | 0.65487        | -0.75849        | 0.13405         | -4.44948        | 0.28149         | 2.37059         | 1.56666         | 4.78108                   |
| 16        | 0.33645        | 0.79789        | 0.95181        | 1.47681        | -1.01417       | 0.65487        | -0.75849        | 0.13405         | -4.44948        | -2.86010        | -2.37059        | -1.57493        | 4.78108                   |



Pose 3 of Fig. 2 (shown in lighter colours) superposed on pose 1 (shown in darker shades) from the same figure. These two branches of FK correspond to the “elbow-up” and “elbow-down” configurations of the RR-chain,  $p_L-p-p_R$

Pose 2 of Fig. 2 (shown in lighter colours) superposed on pose 1 (shown in darker shades) from the same figure. These two branches of FK correspond to a “half-turn” (i.e., rotation through  $\pi$ ) at the passive joints at  $p_L$  and  $p-p_R$ . Table 4 shows that the angles  $\phi_{4L}$  and  $\phi_{4R}$

**Figure 3.** Geometric relations between some of the FK branches shown in Fig. 2. The view angles have been chosen so as to enhance the visual clarity in the 2-D figures.

result in the same physical configuration of the manipulator, as seen in Fig. 4. Thus, one can summarise the situation as having 40 branches of solution, each with two possible configurations of the right arm.

### 5. Numerical examples

In this section, the theoretical developments presented so far are illustrated via numerical examples. The FKP is solved first for a given set of inputs. The resulting pose of the manipulator is used as the input to the IKP, which provides an intrinsic means of validating the results of both. The values of the architecture parameters used are listed in Table III. All the lengths and angles mentioned in this paper are measured in metres and radians, respectively. Real values, such as 0.5 and 2.69, have been replaced by  $\frac{1}{2}$  and  $\frac{269}{100}$ , respectively, to take advantage of the exact arithmetic computations afforded by the CAS employed, as opposed to the default floating-point operations.

#### 5.1. Forward kinematics

The numerical values of the active joint angles are chosen as  $\theta_1 = \frac{\pi}{10}$ ,  $\theta_{2L} = \frac{\pi}{3}$ ,  $\theta_{3L} = \frac{\pi}{6}$ ,  $\theta_{2R} = \frac{\pi}{6}$ ,  $\theta_{3R} = \frac{\pi}{3}$  and  $\theta_7 = \frac{\pi}{4}$ . The values of the passive joint angles obtained are listed in Table IV, and the corresponding poses of the manipulator are depicted in Fig. 2. It is interesting to note that two distinct branches of solutions to the FKP result in *identical* poses of the manipulator (as indicated in the subcaptions in Fig. 2). In other words, mathematically speaking, there are eight branches to the solutions of FKP, which manifest, in the general case, only as four distinct physical poses. This is due to the parametrisation of the passive spherical joint at  $p_R$  in terms of the variables  $\phi_{4R}$ ,  $\phi_{5R}$  and  $\phi_{6R}$ , which correspond to a set of Euler angles, which allow two distinct sets of values to describe the same physical orientation. Specifying the active variables  $\{\theta_1, \theta_{2L}, \theta_{2R}, \theta_{3L}, \theta_{3R}\}$  locates  $p_L$  and  $p_R$  *uniquely* in space. Therefore, the 2-R chain  $p_L-p-p_R$  can be assembled, in general, in two different manners, analogous to the “elbow-up” and “elbow-down” configurations appearing in the IK of planar 2-R manipulators, as seen in the poses 1 (or 5) and 3 (or 7), in Fig. 3(a). These configurations of the chain  $p_L-p-p_R$ , being *mirror-symmetric* about the line  $p_Lp_R$ , share the same plane. This is reflected by the common value of  $\phi_{4L}$  between these two branches (see Table IV), since the orientation of the plane containing the chain  $p_L-p-p_R$  is governed by  $\phi_{4L}$ . As may be expected, these geometric conditions continue to hold good when

the passive joint variable  $\phi_{4L}$  undergoes a change by  $\pm\pi$  starting from its value at pose 1 (or, 3, 5, 7) results in the pose 2 (or 4, 6, 8, respectively), as seen in poses 1 and 2, in Fig. 3(b). The same is reflected in the values of  $\phi_{4L}$ , as seen in Table IV.

Each branch of solution is validated numerically by substituting them back in the original constraint equations, namely Eqs. (6) and (13), and computing their residue as the vector  $\eta_{FK} = [\eta_{FKL}, \eta_{FKR}]^T$ . A scalar measure of error,  $e_{FK}$ , is then introduced via the norm of this residue:

$$e_{FK} = \|\eta_{FK}\|. \quad (80)$$

The solutions are deemed accurate if  $e_{FK} \leq 10^{-10}$ . The last column of Table IV tabulates the actual values of  $e_{FK}$  corresponding to all the branches of solutions.

A Mathematica “demonstration” (i.e., a GUI) has been developed to simulate finite inputs at the active joints and to visualise the corresponding motions via on-screen animation. A simple example is captured in the video file `animation_forward_kinematics_H6A.mp4`, wherein each joint is *jogged*, albeit virtually, over finite ranges of inputs by manipulating individual sliders.

## 5.2. Inverse kinematics

The end-effector pose defined by  $\alpha = 1.19556$ ,  $\beta = 2.27373$ ,  $\gamma = -1.27501$ ,  $p_x = 5.17431$ ,  $p_y = 1.03851$  and  $p_z = 2.72026$ , obtained in the first and fifth branches of forward kinematic solutions in Table IV of Section 5.1, is used as input for performing the IKP.

As mentioned in Section 4, the symbolic expressions of the coefficients of the IKU equation (see (74)) are huge in size (see (75)). Therefore, even though these expressions are exact in nature, the numerical values they yield after substitution of input variables as floating point numbers may incorporate significant error, due to accumulation of truncation errors associated with floating-point arithmetic. Hence, floating-point numbers are replaced by their rational approximations (accurate up to the fifth digit after the decimal), in order to pursue numerical computations in the exact form, to the extent possible. The resulting IKU equation, that is, the numerical version of (74), is expressed in the *monic*<sup>21</sup> form and its coefficients, truncated to the fifth place after the decimal, are presented in Table V.

The IKU equation has been solved using the built-in routine `Solve` of Mathematica.

The values of joint angles corresponding to the real roots of the IKU are listed in Table VI, and the poses of the manipulator corresponding to the branches are shown in Fig. 4. Similar to the solutions of FKP, it may be seen here that a pair branches of mathematical solutions of the IKP result in the same physical pose (see Table VI and Fig. 4). The IKP solutions can also be grouped pairwise into *elbow-up* and *elbow-down* configurations of the right arm, as can be seen, for example, in Fig. 4(a) and (b), respectively, the said elbow joint being located at  $e_R$ .

As in the case of the FKP, a scalar measure of error is defined by referring back to the original constraint equations, namely Eqs. (18) and (25):

$$e_{IK} = \|\eta_{IK}\|. \quad (81)$$

However, due to much greater complexity of computations involved in this case, for example, the solution of the 40-degree IKU equation, the acceptable limit on the error is set at  $e_{IK} \leq 10^{-5}$ . It may be noted that this limit is adequately small for these computations, as it is seen, for example, the inverse kinematic solution branches (9, 10) in Table VI match with the corresponding forward kinematic solution branches, namely (1, 5) in Table IV, up to the fourth place after the decimal. The last column of Table VI lists the measure of error in each branch of solution.

<sup>21</sup>A polynomial/equation is called monic when the leading coefficient equals unity.

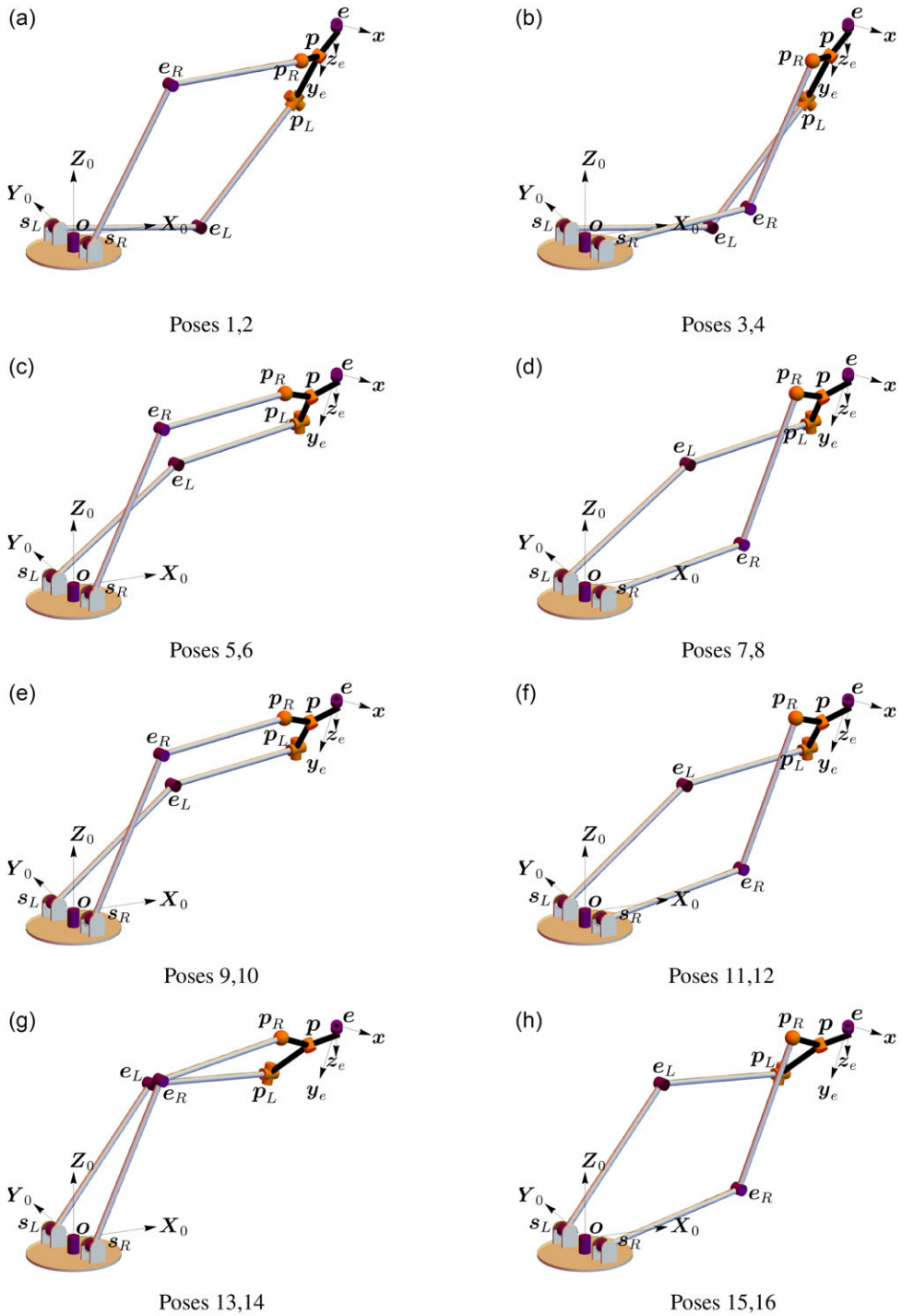


**Figure 4.** Poses depicting the real solutions to the inverse kinematic problem for the given inputs (enumerated as per the rows of Table VI).

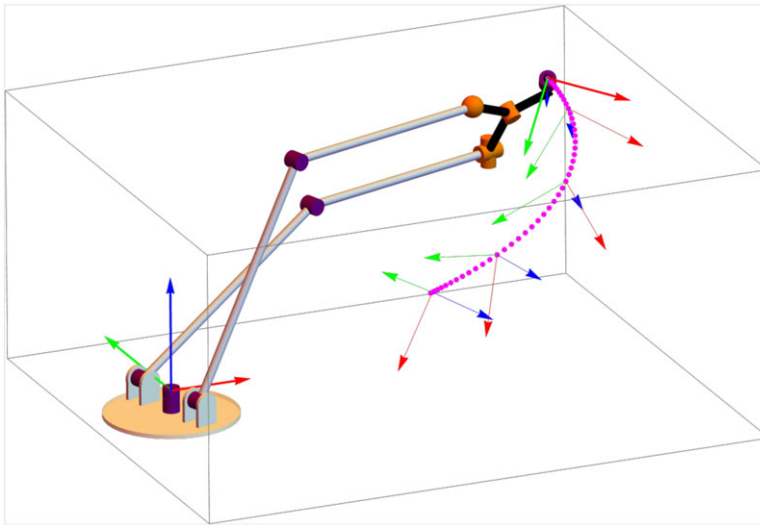


**Figure 5.** A schematic depicting the setup for the trajectory-tracking simulation. The manipulator is depicted at the initial point of the path, which is chosen to be pose 1 shown in Fig. 2(a), conforming to FK branch 1 in Table IV. The path corresponding to this branch of FK, which is computed first as per the actuator inputs given by Eq. (82), is shown by magenta dots. It is subsequently tracked by the manipulator, following the IK branch 9, whose initial point is listed in Table VI. The evolution of the end-effector frame,  $\mathbf{x}_e \mathbf{y}_e \mathbf{z}_e$ , is shown by the triad of mutually orthogonal arrows in the RGB convention, with “R” denoting X, and so on. Only a few sets of target frames are shown to avoid clutter. The simulation has been captured in the video file *animation\_inverse\_kinematics\_H6A.mp4* associated with this paper. (Reference to colours pertain to the digital version of this article.)

**5.3. Forward and inverse kinematics along joint-space trajectories**

In the above, the results obtained in the FK and IK analyses have been validated for their numerical accuracies by evaluating their residues independently, and also by checking one against the other for a given set of inputs. In the following, the same is repeated for a finite span of motion of the manipulator, by making it follow a given trajectory in its active joint space. Without any loss of generality, it is assumed that the manipulator starts from rest and also comes to a complete halt at the end of the trajectory.

The initial configuration of the robot is chosen to be pose 1 shown in Fig. 2(a) that belongs to FK branch 1 in Table IV. The set of active angles in this configuration is denoted by  $\theta_1$ . For the final pose, the active angles, given by  $\theta_F = [\theta_{1F}, \theta_{2LF}, \theta_{2RF}, \theta_{3LF}, \theta_{3RF}, \theta_{7F}]^T = \left[-\frac{7\pi}{30}, \frac{\pi}{6}, 0, \frac{\pi}{2}, \frac{7\pi}{12}, \frac{5\pi}{12}\right]^T$ , are chosen arbitrarily. Nevertheless, care is taken to ensure (by visual inspection) that the links of the manipulator do not interfere while executing this trajectory.

The active joint variables at any time  $t \in [0, T_m]$  are obtained by a *cubic interpolation* of  $\theta_1$  and  $\theta_F$ , subjected to the static end conditions mentioned above:

$$\theta(t) = \theta_1 + \left(3 - \frac{2t}{T_m}\right) \left(\frac{t}{T_m}\right)^2 (\theta_F - \theta_1), \tag{82}$$

where  $T_m$  is the duration of motion. Equation (82) is used to sample  $\theta(t)$  uniformly at  $n$  points ( $n$  being 50 in the present case), to obtain  $n$  sets of inputs to the FK problem, denoted by  $\theta_i = \theta(iT_m/n), i = 1, 2, \dots, n$ . For each  $\theta_i$ , FK is performed following the solution procedure presented in Section 3 to determine the end-effector coordinates,  $\mathbf{X}_i = [x_i, y_i, z_i, \alpha_i, \beta_i, \gamma_i]$ . All the passive angles are also computed in the process. The variations in the angles  $\phi_{4L}, \phi_{4R}, \phi_{5L}, \phi_{5R}, \phi_{6L}$  and  $\phi_{6R}$  w.r.t. time are plotted in Fig. 6. Among the eight FK branches obtained for each  $\theta_i$ , only the first branch (i.e., corresponding to the first

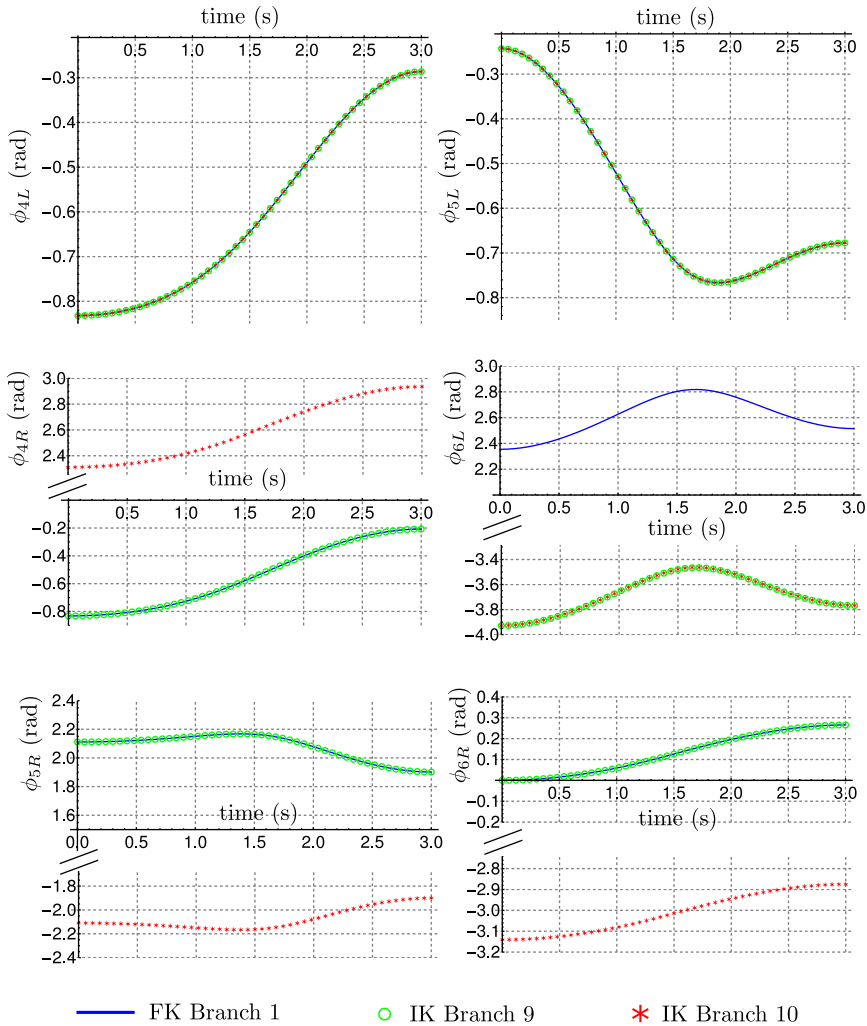


**Figure 6.** Variations of the passive joint angles with time, as obtained from forward and inverse kinematic analysis. The IK branch 9 retraces the FK branch 1, as expected, the apparent mismatch in the values of  $\phi_{6L}$  being due to a difference of  $2\pi$ , which is trivial. It may also be noted that in the cases of  $\phi_{4R}$  and  $\phi_{6R}$ , IK branch 10 differs from the IK branch 9 by  $\pi$ , while they have the opposite signs in the case of  $\phi_{5L}$ .

row in Table IV) is considered at all the time instances, since the initial pose corresponds to this branch. These plots provide the references for the IK solutions to be validated.

Inverse kinematic analysis is performed next, using as inputs the end-effector coordinates,  $X_i$ , found in the FK process. From Table VI, it may be seen that the initial pose corresponds to the 9th branch of the IK solutions, making it the obvious choice for tracking and superposing the results in Fig. 6. As expected, this branch of IK agrees at all the points with the reference, that is, FK branch 1. Another branch of IK, namely the 10th, is also included in the said figure. While this branch is not supposed to match the reference trajectories in all the variables, it has certain interesting relations with it, as noted in the caption of Fig. 6.

Computationally, the tracking of the different IK branches is achieved by solving Eqs. (32)–(37) at each point  $X_i$  using the routine FindRoot available in Mathematica. It uses an iterative technique, and it is found that the IK solution at the previous point,  $X_{i-1}$ , serves as a successful initial guess

while computing  $X_i$  in all the instances. These computations, as summarised visually in Fig. 6, provide conclusive validations of the computational methods proposed in this article, and the results obtained thereof.

In the next section, the singularity conditions obtained while solving the FKP and IKP, in Sections 3, 4, respectively, are studied in detail.

### 6. Analysis of singularities in the forward and inverse kinematics

The analysis of loop-closure equations of a manipulator leads to the solution of its FKP and IKP, as seen in the previous sections. In this section, the special cases identified in that process, that is, poses at which pairs of branches of solutions merge, are discussed in detail.

It is helpful to initiate this discussion considering the general case first. Therefore, the loop-closure constraints in Eqs. (19)–(25) and Eqs. (26)–(31) are represented as:

$$\mathbf{g}(\boldsymbol{\theta}, \boldsymbol{\phi}, \mathbf{x}) = \mathbf{0}, \quad \boldsymbol{\theta}, \boldsymbol{\phi}, \text{ and } \mathbf{x} = [x, y, z, \alpha, \beta, \gamma]^\top \in \mathbb{R}^6, \quad \mathbf{g} \in \mathbb{R}^{12}. \tag{83}$$

Differentiating (83) with respect to time,  $t$ , one obtains

$$\frac{d\mathbf{g}}{dt} = \frac{\partial \mathbf{g}}{\partial t} + \frac{\partial \mathbf{g}}{\partial \mathbf{x}} \dot{\mathbf{x}} + \frac{\partial \mathbf{g}}{\partial \boldsymbol{\theta}} \dot{\boldsymbol{\theta}} + \frac{\partial \mathbf{g}}{\partial \boldsymbol{\phi}} \dot{\boldsymbol{\phi}} = \mathbf{0}. \tag{84}$$

In the case of the H6A manipulator, the constraint equations are *scleronomic* (see, e.g., ref. [27], pp. 74), that is, they have no explicit dependence on time. Hence, (84) reduces to (85), which relates the output velocity,  $\dot{\mathbf{x}}$ , to the input velocity,  $\dot{\boldsymbol{\theta}}$ , and the passive joint velocity,  $\dot{\boldsymbol{\phi}}$ :

$$\mathbf{J}_{g\mathbf{x}} \dot{\mathbf{x}} + \mathbf{J}_{g\boldsymbol{\theta}} \dot{\boldsymbol{\theta}} + \mathbf{J}_{g\boldsymbol{\phi}} \dot{\boldsymbol{\phi}} = \mathbf{0}, \quad \text{where } \mathbf{J}_{g\mathbf{x}} := \frac{\partial \mathbf{g}}{\partial \mathbf{x}}, \mathbf{J}_{g\boldsymbol{\theta}} := \frac{\partial \mathbf{g}}{\partial \boldsymbol{\theta}}, \mathbf{J}_{g\boldsymbol{\phi}} := \frac{\partial \mathbf{g}}{\partial \boldsymbol{\phi}} \in \mathbb{R}^{12 \times 6}. \tag{85}$$

There are many definitions and corresponding classifications of kinematic singularities. In the following, two types of singularities would be discussed, following refs. [28], [29], namely the *loss-* and the *gain-type* of singularities. The loss-type singularity is defined here w.r.t. the end-effector, which loses one or more DoF at such a singularity. The gain-type singularity, as the name suggests, leads to a gain of one or more DoF, which manifests either at the end-effector or at some other passive link(s), or both.

- Loss-type singularities: The loss-type singularity occurs when a non-zero input fails to produce any output at the end-effector, that is,  $\dot{\boldsymbol{\theta}} \neq \mathbf{0}$  but  $\dot{\mathbf{x}} = \mathbf{0}$ . Therefore, (85) reduces to:

$$\mathbf{J}_{g\boldsymbol{\theta}} \dot{\boldsymbol{\theta}} + \mathbf{J}_{g\boldsymbol{\phi}} \dot{\boldsymbol{\phi}} = \mathbf{0}; \tag{86}$$

$$\Rightarrow \mathbf{J}_{g\mathbf{q}} \dot{\mathbf{q}} = \mathbf{0}, \quad \text{where } \mathbf{J}_{g\mathbf{q}} := [\mathbf{J}_{g\boldsymbol{\theta}} \ \mathbf{J}_{g\boldsymbol{\phi}}] \in \mathbb{R}^{12 \times 12} \text{ and } \mathbf{q} = [\boldsymbol{\theta}^\top, \boldsymbol{\phi}^\top]^\top.$$

Since  $\dot{\boldsymbol{\theta}} \neq \mathbf{0}$  (as mentioned above),  $\dot{\mathbf{q}} \neq \mathbf{0}$ , too. Hence, the condition for loss-type singularity is obtained as:

$$\det(\mathbf{J}_{g\mathbf{q}}) = 0. \tag{87}$$

It may be noted that (86) may be satisfied even when  $\dot{\mathbf{x}} \neq \mathbf{0}$ , iff  $\mathbf{J}_{g\mathbf{x}}$  is also singular, and  $\dot{\mathbf{x}} \in \text{nullspace}(\mathbf{J}_{g\mathbf{x}})$ .

- Gain-type singularities: The manipulator is said to encounter a gain-type singularity when the end-effector and/or the passive link(s) acquire an infinitesimal or finite motion capability, that is, either  $\dot{\mathbf{x}} \neq \mathbf{0}$  or  $\dot{\boldsymbol{\phi}} \neq \mathbf{0}$ , or both, even when the actuators are held fixed, that is,  $\dot{\boldsymbol{\theta}} = \mathbf{0}$ . Therefore, at a gain-type singularity, (85) reduces to:

$$\mathbf{J}_{g\xi} \dot{\xi} = \mathbf{0}, \quad \text{where } \xi = [\mathbf{x}^\top, \boldsymbol{\phi}^\top]^\top, \text{ and hence, } \mathbf{J}_{g\xi} := [\mathbf{J}_{g\mathbf{x}} \ \mathbf{J}_{g\boldsymbol{\phi}}] \in \mathbb{R}^{12 \times 12}. \tag{88}$$

Since  $\dot{\xi} \neq \mathbf{0}$  as at least one of  $\dot{x}$  and  $\dot{\phi}$  is/are non-zero, the condition for gain-type singularities may be derived as:

$$\det(\mathbf{J}_{g\xi}) = 0. \tag{89}$$

As in the case of loss-type singularities, in this case, (88) holds good for  $\dot{\theta} \neq \mathbf{0}$ , iff  $\mathbf{J}_{g\theta}$  is also singular, and  $\dot{\theta} \in \text{nullspace}(\mathbf{J}_{g\theta})$ .

Furthermore, the manipulator encounters loss-type and gain-type singularities simultaneously in the case when  $\mathbf{J}_{gq}\dot{q} = \mathbf{0}$  and  $\mathbf{J}_{g\xi}\dot{\xi} = \mathbf{0}$  together, that is,  $\det(\mathbf{J}_{gq}) = 0$  (see (87)) and  $\det(\mathbf{J}_{g\xi}) = 0$  (see (89)).

The singularities observed during the analyses of the FKP and the IKP are explained in the context of loss and gain of DoF in the following. Certain *architecture singularities* (i.e., special architectures, at which all poses can be singular in one or more ways) also appeared in the course of the mathematical analysis. Some of these are trivial in nature, for example, those which require the vanishing of the parameters  $l_2, l_3, l_w$ , which are ignored as these are not feasible physically. Some others are of practical interest, and these have been discussed in detail in the appropriate context.

### 6.1. Singularity conditions arising out of forward kinematic analysis

The singularity conditions gleaned from the study of the FKP are revisited in this subsection. The specific cases are enumerated hereafter.

- Case 1:  $\sin \frac{\phi_{6L}}{2} = 0$  or  $\sin \left( \phi_{5L} + \frac{\phi_{6L}}{2} \right) = 0$ . It is noticed that either of the conditions  $\sin \frac{\phi_{6L}}{2} = 0$  or  $\sin \left( \phi_{5L} + \frac{\phi_{6L}}{2} \right) = 0$  leads to the architecture singularity of  $d_2 = 0$  (see (6)), which causes simultaneous rank deficiency of the Jacobian matrices  $\mathbf{J}_{gq}$  and  $\mathbf{J}_{g\xi}$ . However, this singularity is not relevant for the H6A manipulator, as its architecture ensures that the two arms always lie in *parallel* planes at a mutual distance of  $2d_2 > 0$  (see Table III).
- Case 2:  $\sin \phi_{5R} = 0$ . It is interesting to note that this condition is akin to that of *gimbal lock* in the context of Euler angles, due to the representation of the spherical joint, leading to a loss-type singularity. This singularity is analogous to the “wrist singularity” associated with the *wrist-decoupled* 6-R spatial manipulators, such as PUMA 560 (see, e.g., ref. [1], pp. 79). The condition  $\sin \phi_{5R} = 0$  leads to at least one of the two following conditions (refer to (13)):  $\cos \phi_{4L} = 0$ , and  $\sin(\phi_{5L} + \phi_{6L}) = 0$ , which are discussed separately in the following.
  1.  $\cos \phi_{4L} = 0$ . The condition  $\cos \phi_{4L} = 0$ , together with  $\sin \phi_{5R} = 0$ , yet again yields the architecture singularity  $d_2 = 0$  (see (6)) and results in the degeneracy of  $\mathbf{J}_{gq}$  and  $\mathbf{J}_{g\xi}$ .
  2.  $\sin(\phi_{5L} + \phi_{6L}) = 0$ . In this case, too, the Jacobian matrices  $\mathbf{J}_{gq}$  and  $\mathbf{J}_{g\xi}$  lose rank, leading to a coincidence of the gain- and loss-type of singularities. As may be seen in Fig. 7(a), the links  $\mathbf{p}_L\mathbf{p}$  and  $\mathbf{p}\mathbf{p}_R$  become collinear indicating the merger of two configurations of the sub-chain  $\mathbf{p}_L\mathbf{p}\mathbf{p}_R$  which would lie on either side of the line  $\mathbf{p}_L\mathbf{p}_R$  in the absence of this singularity. It may be verified that the point  $\mathbf{p}$  gains an infinitesimal translational DoF along a line perpendicular to both the line  $\mathbf{p}_L\mathbf{p}_R$  and the axis of the passive rotary joint at  $\mathbf{p}$ . This DoF is independent of all the actuators.

### 6.2. Singularity conditions arising out of inverse kinematic analysis

The physical significance of the singularity conditions obtained from the study of the IKP is studied in this subsection. The specific cases are listed below.

- Case 1:  $i_1^2 + j_1^2 - k_1^2 = 0$  and  $i_2^2 + j_2^2 - k_2^2 = 0$  (see Eqs. (40) and (41), respectively). When these conditions are satisfied simultaneously, the compound variable  $(\phi_{5L} + \psi_{6L})$  appears in identical

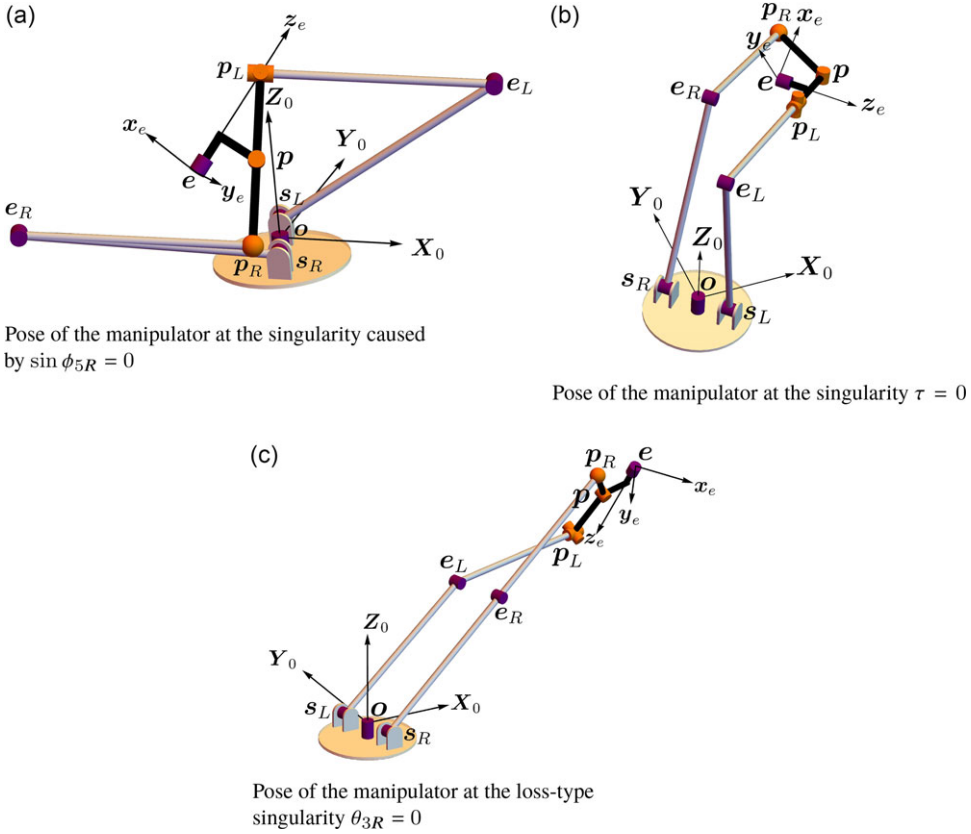


**Figure 7.** The joint angles of the pose in Fig. 7(a) are  $\theta_1 = 0.31416, \theta_{2L} = 1.04720, \theta_{3L} = -2.48784, \theta_{2R} = -1.40982, \theta_{3R} = -3.17242, \theta_7 = 0.78540, \phi_{4L} = -1.04720, \phi_{5L} = 0, \phi_{6L} = 3.14159, \phi_{4R} = 1.04720, \phi_{5R} = 0$  and  $\phi_{6R} = 3.14159$  and the architecture parameters are mentioned in Table III. For Fig. 7(b), the joint angles are  $\theta_1 = -2.35619, \theta_{2L} = 0.12378, \theta_{3L} = 4.29217, \theta_{2R} = -0.46959, \theta_{3R} = 4.80511, \theta_7 = -2.32155, \phi_{4L} = -3.14159, \phi_{5L} = 1.57080, \phi_{6L} = -2.09440, \phi_{4R} = 3.00331, \phi_{5R} = 0.52917$  and  $\phi_{6R} = 0.15984, l_w = 1.1547$  and the rest of the architecture parameters is mentioned in Table III. Similarly, the poses of the manipulator in Fig. 7(c) are for the joint angles  $\theta_1 = 0.31416, \theta_{2L} = 1.04720, \theta_{3L} = 0.52360, \theta_{2R} = 1.01576, \theta_{3R} = 0, \theta_7 = 0.78540, \phi_{4L} = -0.98233, \phi_{5L} = 0.13389, \phi_{6L} = 2.38188, \phi_{4R} = 0.04002, \phi_{5R} = 2.81015$  and  $\phi_{6R} = 1.11732$  and the architecture parameters are mentioned in Table III.

pairs in the solutions of IKP of the manipulator. It is interesting to note that the condition,  $\tau = 0$  (see (71)), exemplifies such a situation, which, in turn, has the following consequences:

$$\tau = 0 \Rightarrow \begin{cases} \cos \theta_{\alpha_1} = 0, \\ \cos \beta \sin \theta_{\alpha_1} = 0. \end{cases} \tag{90}$$

Both the Jacobian matrices  $J_{gq}$  and  $J_{g\xi}$  lose rank under these conditions. Figure 7(b) shows an example of such a singularity, in which it is observed that the loss of a DoF is attributed to the fact that the axis of active rotary joint at  $e$  is parallel to those of the other active rotary joints on the left chain, namely  $s_L$  and  $e_L$ . It is also found that these conditions lead to the vanishing of  $\psi_{6L}$  and, finally, forms an architecture singularity, given by:

$$l_w \sin \kappa = 2d_2. \tag{91}$$

As long as this condition is satisfied, this kind of singularity would occur on a finite-dimensional subspace of the workspace of the manipulator.

- Case 2:  $a_1b_2 - a_2b_1 = 0$  (refer to (47)). It may be observed that the condition  $a_1b_2 - a_2b_1 = 0$  is trivially satisfied when  $a_1 = 0$  and  $b_1 = 0$ , which also make  $\mu$  vanish as per (48). In (44),  $a_1 = \sin \beta \sin \theta_{\gamma}$  and  $b_1 = -(\cos \theta_{\gamma} \sin \theta_{\alpha_1} + \cos \beta \cos \theta_{\alpha_1} \sin \theta_{\gamma})$ . Hence, vanishing of  $a_1, b_1$  simultaneously leads to two subcases: (a)  $\beta = 0, \theta_{\alpha_1} = -\theta_{\gamma}$  and (b)  $\theta_{\alpha_1} = 0, \theta_{\gamma} = 0$ . The former subcase is equivalent to gimbal lock at the end-effector due to the representation of the orientation using Euler angles. This is a parametric singularity and has been mentioned previously in Case 2 in Section 6.2. Interestingly, both the subcases result in a loss-type singularity, as seen in the loss of rank of  $\mathbf{J}_{gq}$ , and also lead to the architecture singularity,  $d_2 = 0$ . However, in this case, the architecture singularity is not associated with a coincidence of loss-type and gain-type of singularities, as in the Cases 1 and 2 discussed previously in Section 6.1.
- Case 3:  $a_2^2 + b_2^2 - c_2^2 = 0$  (see (45)). This singularity corresponds to the merging of the *elbow-up* and *elbow-down* configurations of the planar 2-R sub-chain  $s_L \mathbf{e}_L - \mathbf{e}_L \mathbf{p}_L$ , as evidenced by the vanishing of  $\sin \theta_{3L}$  and the consequent loss of rank of  $\mathbf{J}_{gq}$ . In this case, the point  $\mathbf{p}_L$  loses its ability to translate along the direction of the links  $s_L \mathbf{e}_L$  and  $\mathbf{e}_L \mathbf{p}_L$ .
- Case 4:  $b_3^2 - 4a_3c_3 = 0$  and  $b_4^2 - 4a_4c_4 = 0$  (refer to Eqs. (54) and (55), respectively). If satisfied simultaneously, these conditions force a pair of values of the variable  $\psi_{6L}$  to merge in the solutions of IKP of the manipulator, causing a singularity in the matrix  $\mathbf{J}_{gq}$  and consequently, the loss of a DoF. Interestingly, this case is observed to be satisfied when  $\mu = 0$  (see (48)), which requires vanishing of  $d_2$ , just as in Case 2 above.
- Case 5:  $\Delta_1 = 0$  and  $b_5^2 - 4a_5c_5 = 0$  (see Eqs. (67) and (68), respectively). In this case, variable  $\theta_{\gamma}$  acquires a pair of repeated values in the solution of the IKP of the manipulator, resulting in a loss-type singularity. This is also reflected in the singularity of the Jacobian matrix  $\mathbf{J}_{gq}$ .
- Case 6:  $\Delta_2 = 0$  (see (76)). This condition corresponds to the merger of the solutions of the variable  $\theta_{\alpha_1}$ , leading to a loss-type singularity, as reflected in the rank deficiency of the Jacobian matrix  $\mathbf{J}_{gq}$ .
- Case 7:  $o_1^2 + o_2^2 - o_3^2 = 0$  (refer to (79)). This condition indicates the merger of the *elbow-up* and *elbow-down* configurations of the 2-R sub-chain  $s_R \mathbf{e}_R - \mathbf{e}_R \mathbf{p}_R$  which causes  $\sin \theta_{3R}$  to vanish. It is obvious (see Fig. 7(c)) that in this case the point  $\mathbf{p}_R$  cannot have any motion along the said links for any combination of actuator inputs. As expected, this loss of DoF is confirmed by the degeneracy of the matrix  $\mathbf{J}_{gq}$ .

### 7. Discussions

As mentioned before, the kinematics of the H6A is significantly challenging because of two reasons: (a) incorporation of multi-DoF passive joints in its architecture and (b) the asymmetry of the two limbs constituting the manipulator – while the left arm has a universal joint just before the wrist assembly, the right one has a spherical joint. Interestingly, in this case, the IKP is much more complicated than the FKP. Therefore, these two problems are addressed in a manner which is found to be best suited for them individually, starting from different sets of equations depicting the kinematic constraints. This approach is perhaps not the most common in the kinematic analyses of hybrid and parallel robots.

The solution to the FKP has only eight branches, all of which could be obtained in the closed form (see Section 3). The IKP has 160 solutions, which were obtained by first reducing the problem to the solution of a univariate polynomial equation of degree 40, as shown in Section 4. While this approach of reducing a set of simultaneous loop-closure equations to a univariate equation of higher degree is indeed common in manipulator kinematics, a significant distinction of the computational approach presented in this paper vis-à-vis most others is that *the coefficients of the said polynomial were obtained as closed-form symbolic expressions in terms of the original inputs, that is, the pose variables  $\{x, y, z, \alpha, \beta, \gamma\}$* . In doing so, it is ensured that the results obtained are *fully generic* over the workspace of the manipulator. It is, therefore, established conclusively that the *H6A manipulator has 160 solutions for the IKP in the complex plane, and 8 for the FKP, for any possible set of inputs.*

Another useful consequence of the exact symbolic approach is that *all* the *special* configurations associated with the FKP and IKP are identified analytically. At these configurations, there are certain breakdowns in the solution procedure arising out of the merger of different branches of kinematics. Such configurations are analysed further to categorise them into loss-type, gain-type and architecture singularities (see Section 6). Most of the architecture singularities requiring certain link lengths to vanish are avoided naturally, as in the actual manipulator these lengths are not zeros (see Case 1 in Section 6.1 and Cases 2 and 4 in Section 6.2). However, in Case 1 discussed in Section 6.2, a very important condition is derived, which is non-trivial in nature, namely Eq. (91). It shows that the architecture parameters  $d_2$ ,  $l_w$  and  $\kappa$  *cannot be chosen arbitrarily*, but in a manner so as *not* to satisfy (91). It turns out that for the given values of  $d_2$  and  $\kappa$  in Table III, this architecture singularity occurs at  $l_w = 1.1547$ , which is distinct from the actual architecture of the manipulator, where  $l_w = 1$ , but not very far from it.

It may be mentioned here that the closed-form analytical results summarised above could only be derived at the cost of a huge amount of symbolic computations and several improvisations, the details of which may be found in Section 4. Specially designed algorithms to simplify large expressions constituted of trigonometric and algebraic subexpressions were employed in these computations, since a direct application of the default general-purpose routines of the CAS used proved to be grossly inadequate for this purpose. In particular, the elimination of the variables  $\psi_{6L}$  and  $\theta_{7r}$  from Eqs. (20), (48) and Eqs. (27), (60), respectively, demanded a customised approach, involving careful observation and exploitation of the special structures appearing in some expressions, specifically:

- Deriving (48) from (46) by rearranging and taking square roots brought down the size of the equation  $p = 0$  in (53) from 6.110 MB to 19.232 KB
- Using the identities in (61) facilitated:
  - downsizing of the equation  $u_1 = 0$  (refer to (64)) from 191.635 MB to 79.873 MB, and
  - the factoring of  $\sin^2 \theta_{\alpha_1}$  in (73), thereby the reduction in degree of the IKU by 4
- Rewriting the polynomial equations as shown in (69) and (70) enabled the factoring of the polynomial  $\tau$  (see (72)) and dropped the degree of the IKU by 8. Moreover, it also led to the identification of the singularity caused by the vanishing of the polynomial  $\tau$ .

Even with these computational concoctions, the sizes of the final expressions, for example the coefficients of the univariate polynomial representing the IKP, sum up to 2760.873 GB. Without these customised tools and improvisations, it may not have been possible to derive these expressions in the closed form.

These symbolic computations, leading to the derivation of the univariate polynomial equation representing the IKP and the analysis of the singularities associated with the FKP and IKP, form the contributions of this paper.

## 8. Conclusions

This paper presents a comprehensive study of a novel six-DoF spatial manipulator of hybrid architecture named H6A. The manipulator has two arms originating from a rigid “waist” which can swivel about a fixed vertical axis. The arms join at the other end to form a wrist assembly. Asymmetry in the architecture of the arms due to the presence of different multi-DoF passive joints in each makes the kinematics of the manipulator complicated enough to be of sufficient interest. While the FKP is solved easily to obtain all the eight solutions in the closed form, the IKP proves to be much harder, with a total of 160 solutions in the general case. Through extensive symbolic computations, this problem is reduced to that of solving a 40-degree polynomial equation. The coefficients of this polynomial are obtained as closed-form symbolic expressions of the corresponding inputs, which establishes the generic nature of the solutions. The results obtained are numerically validated by computing the residues of the original equations, as well as using the solutions of the forward kinematics in the inverse kinematics. The symbolic nature

of the analysis presented in the paper affords the identification of the associated singularities in a natural manner, that is, by obtaining the conditions for the merger of the kinematic branches. This exact symbolic computation approach to kinematic analysis may be helpful in studying other hybrid/parallel manipulators.

**Supplementary material.** To view supplementary material for this article, please visit <https://doi.org/10.1017/S0263574723000334>.

**Acknowledgements.** The authors thank Dr Jagannath Raju, CTO, and Mr Sharachchandra Bhat, ex-employee, Systemantics India Pvt. Ltd., Bengaluru, India, for sharing with them the architecture data listed in Table III. They also thank Mr Bibekananda Patra, doctoral student at the Department of Engineering Design, Indian Institute of Technology Madras, for creating the GUI demonstrating the forward kinematics and the corresponding video.

**Author contributions.** The problem statement was perceived by PG and SB. The analysis and computations were performed by PG and SR, under the guidance of SB. The paper was written by PG, SR and SB.

**Financial support.** This research received no specific grant from any funding agency, commercial or not-for-profit sectors.

**Competing interest.** The authors declare no conflicts of interest exist.

**Ethical standards.** Not applicable under the heading.

## References

- [1] A. Ghosal, *Robotics: Fundamental Concepts and Analysis* (Oxford University Press, New Delhi, 2006).
- [2] K. Waldron, M. Raghavan and B. Roth, "Kinematics of a hybrid series-parallel manipulation system," *ASME J. Dynam. Syst. Meas. Control* **111**(2), 211–221 (1989).
- [3] M. Shahinpoor, "Kinematics of a parallel-serial (hybrid) manipulator," *J. Field Robot.* **9**(1), 17–36 (1992).
- [4] D. Chablat, P. Wenger and J. Angeles, "The Kinematic Design of a 3-DoF Hybrid Manipulator," **In: *Integrated Design and Manufacturing in Mechanical Engineering '98*** (1999) pp. 225–232.
- [5] T. Tanev, "Kinematics of a hybrid (parallel-serial) robot manipulator," *Mech. Mach. Theory* **35**(9), 1183–1196 (2000).
- [6] L. Romdhane, "Design and analysis of a hybrid serial-parallel manipulator," *Mech. Mach. Theory* **34**(7), 1037–1055 (1999).
- [7] F. Tahmasebi and L. Tsai, "Closed-form direct kinematics solution of a new parallel minimanipulator," *J. Mech. Des.* **116**(4), 1141–1147 (1994).
- [8] S. Rao and J. Raju, "Forward and Inverse Kinematics of a Hybrid Series-parallel Manipulator," **In: *Proceedings of the 15th National Conference on Machines and Mechanisms (NaCoMM 2011)***, Madras (2011) pp. 429–437.
- [9] G. Carbone, M. Ceccarelli and M. Teolis, "A Numerical Evaluation of the Stiffness of CaHyMan (Cassino Hybrid Manipulator)," **In: *2nd Workshop on Computational Kinematics (CK 2001)*** (2001) pp. 145–154.
- [10] J. Gallardo-Alvarado, "Kinematics of a hybrid manipulator by means of screw theory," *Multibody Syst. Dyn.* **14**, 345–366 (2005).
- [11] J. Shi, X. Zhu and Z. Li, "New Method for Kinematic Analysis of a Hybrid Manipulator," **In: *2009 International Conference on Information And Automation*** (2009) pp. 207–211.
- [12] B. Hu, J. Zhao and H. Cui, "Terminal constraint and mobility analysis of serial-parallel manipulators formed by 3-RPS and 3-SPR PMs," *Mech. Mach. Theory* **134**, 685–703 (2019).
- [13] B. Hu, Y. Huo, J. Gao and D. Zhang, "CGA-based approach for the inverse displacement of serial-parallel manipulators," *Mech. Mach. Theory* **176**, 105011 (2022).
- [14] B. Hu, J. Yu, Y. Lu, C. Sui and J. Han, "Statics and stiffness model of serial-parallel manipulator formed by k parallel manipulators connected in series," *J. Mech. Robot.* **4**(2), 021012 (2012).
- [15] W. Guo, R. Li, C. Cao and Y. Gao, "Kinematics Analysis of a Novel 5-DoF Hybrid Manipulator," *Int. J. Automat. Technol.* **9**(6), 765–774 (2015).
- [16] B. Hu, Y. Shi, L. Xu and P. Bai, "Reconsideration of terminal constraint/mobility and kinematics of 5-DOF hybrid manipulators formed by one 2R1T PM and one RR SM," *Mech. Mach. Theory* **149**, 103837 (2020).
- [17] H. Ye, D. Wang, J. Wu, Y. Yue and Y. Zhou, "Forward and inverse kinematics of a 5-DOF hybrid robot for composite material machining," *Robot Comput.-Integr. Manuf.* **65**, 101961 (2020).
- [18] A. Antonov, A. Fomin, V. Glazunov, S. Kiselev and G. Carbone, "Inverse and forward kinematics and workspace analysis of a novel 5-DOF (3T2R) parallel-serial (hybrid) manipulator," *Int. J. Adv. Robot. Syst.* **18**(2), 1729881421992963 (2021).
- [19] Q. Liu and T. Huang, "Inverse kinematics of a 5-axis hybrid robot with non-singular tool path generation," *Robot. Comput.-Integr. Manuf.* **56**, 140–148 (2019).

- [20] G. Yang, I. M. Chen, S. H. Yeo and W. Lin, "Design and analysis of a modular hybrid parallel-serial manipulator for robotised deburring applications," *Smart Dev. Mach. Adv. Manufact.* **65**, 167–188 (2008).
- [21] P. Xu, C. Cheung, B. Li, L. Ho and J. Zhang, "Kinematics analysis of a hybrid manipulator for computer controlled ultra-precision freeform polishing," *Robot Comput.-Integr. Manuf.* **44**, 44–56 (2017).
- [22] S. Kucuk and B. Gungor, "Inverse Kinematics Solution of a New Hybrid Robot Manipulator Proposed for Medical Purposes," *In: 2016 Medical Technologies National Congress (TIPTEKNO)* (2016) pp. 1–4.
- [23] A. Singh, E. Singla, S. Soni and A. Singla, "Kinematic modeling of a 7-degree of freedom spatial hybrid manipulator for medical surgery," *Proc. Inst. Mech. Eng. H: J. Eng. Med.* **232**, 12–23 (2018).
- [24] S. Bandyopadhyay and A. Ghosal, "Geometric characterization and parametric representation of the singularity manifold of a 6-6 Stewart platform manipulator," *Mech. Mach. Theory* **41**(11), 1377–1400 (2006).
- [25] M. L. Husty, "An algorithm for solving the direct kinematics of general Stewart-Gough platforms," *Mech. Mach. Theory* **31**(4), 365–379 (1996).
- [26] D. R. Walter, M. L. Husty and M. Pfurner, "A complete kinematic analysis of the SNU 3-UPU parallel robot," *Contemp. Math.* **496**, 331 (2009).
- [27] F. E. Udwardia and R. E. Kalaba. *Analytical Dynamics: A New Approach* (Cambridge University Press, New York, 2007).
- [28] A. Ghosal and B. Ravani, "A differential-geometric analysis of singularities of point trajectories of serial and parallel manipulators," *J. Mech. Des.* **123**(1), 80–89 (2001).
- [29] S. Bandyopadhyay and A. Ghosal, "Analysis of configuration space singularities of closed-loop mechanisms and parallel manipulators," *Mech. Mach. Theory* **39**(5), 519–544 (2004).
- [30] M. Shoham and B. Roth, "Connectivity in open and closed loop robotic mechanisms," *Mech. Mach. Theory* **32**(3), 279–293 (1997).
- [31] Wolfram Research, Inc., *Mathematica Version 12.0*, Champaign, Illinois (2019).
- [32] D. J. Bates, J. D. Hauenstein, A. J. Sommese and C. W. Wampler, "Bertini," *Version 1.6* (Software for Numerical Algebraic Geometry (2018)).
- [33] S. Qiu and M. R. Lermani, "Precision grasp using an arm-hand system as a hybrid parallel-serial system: A novel inverse kinematics solution," *IEEE Robot. Automat. Lett.* **6**(4), 8530–8536 (2021).

## A. Calculation of the degree-of-freedom of the H6A manipulator

As stated in ref. [30], the mobility of a mechanism with closed loops, that is, the DoF, attributed to both Grübler and Kutzbach, is defined by:

$$M = \sum_{i=1}^p f_i - 6l. \quad (\text{A1})$$

In the above equation,  $l$  is the total number of independent loops,  $p$  is the total number of joints and  $f_i$  is the DoF of the  $i$ th joint. The H6A manipulator consists of one independent kinematic loop  $o-s_L-e_L-p_L-p_R-e_R-s_R-o$ , therefore,  $l = 1$ . The DoF corresponding to all the joints are tabulated in Table A1. Thereafter, substituting data from Table A1 gives  $M = 6$ .

**Table A1.** *Joints of the H6A manipulator and their corresponding DoF.*

| Joint                                 | $f_i$ (DoF) |
|---------------------------------------|-------------|
| Waist, $o$                            | 1           |
| Left shoulder, $s_L$                  | 1           |
| Left elbow, $e_L$                     | 1           |
| Universal joint, $p_L$                | 2           |
| Rotary joint at wrist point, $p$      | 1           |
| Spherical joint, $p_R$                | 3           |
| Right elbow, $e_R$                    | 1           |
| Right shoulder, $s_R$                 | 1           |
| Rotary joint before end-effector, $e$ | 1           |